Lawrence Berkeley National Laboratory

Title
A review of Ni-based layered oxides for rechargeable Li-ion batteries

Permalink
https://escholarship.org/uc/item/9sc716dn

Journal

ISSN

Authors
Xu, Jing
Lin, Feng
Doeff, Marca M
et al.

Publication Date
2017

DOI

Peer reviewed

A Review of Ni-based Layered Oxides for Rechargeable Li-ion Batteries

Journal:	*Journal of Materials Chemistry A*
Manuscript ID	Draft
Article Type:	Review Article
Date Submitted by the Author:	n/a
Complete List of Authors:	Xu, Jing; Lawrence Berkeley National Laboratory, Energy Storage and Distributed Resources Lin, Feng; Lawrence Berkeley National Laboratory, Energy Storage and Distributed Resources Doeff, Marca; Lawrence Berkeley National Laboratory, Energy Storage and Distributed Resources Tong, Wei; Lawrence Berkeley National Laboratory, Energy Storage and Distributed Resources

SCHOLARONE™
Manuscripts

Journal Name

ARTICLE

A Review of Ni-based Layered Oxides for Rechargeable Li-ion Batteries

Jing Xu,‡ [a] Feng Lin,§ [a] Marca M. Doeff, [a] Wei Tong* [a]

The portable electronic market, vehicle electrification (electric vehicles or EVs) and grid electricity storage impose strict performance requirements on Li-ion batteries, the energy storage device of choice, for these demanding applications. Higher energy density than currently available is needed for these batteries, but a limited choice of materials for cathodes remains a bottleneck. Layered lithium metal oxides, particularly those with high Ni content, hold the greatest promise for high energy density Li-ion batteries because of their unique performance characteristics as well as for cost and availability considerations. In this article, we review Ni-based layered oxide materials as cathodes for high-energy Li-ion batteries. The scope of the review covers an extended chemical space, including traditional stoichiometric layered compounds and those containing two lithium ions per formula unit (with potentially even higher energy density), primarily from a materials design perspective. In-depth understanding of the composition-structure-property map for each class of materials will be highlighted as well. The ultimate goal is to enable the discovery of new battery materials by integrating known wisdom with new principles of design, and unconventional experimental approaches (e.g., combinatorial chemistry).

1. Introduction

Rechargeable lithium-ion batteries (LIBs) have become the dominant power sources for portable electronic devices because of their high gravimetric and volumetric energy densities. They are considered the most promising energy storage devices for electric vehicles (EVs), and are now used in vehicles made by Nissan (Leaf) and Tesla, among many others.[1] Mass adoption of EVs is still hindered by insufficient battery performance and high cost. In a Li-ion cell, Li ions shuttle between the positive and negative electrodes, where the redox reactions occur. Currently, the most commonly used anode, graphite, can deliver a much higher specific capacity (372 mAh/g) than available cathodes. Therefore, the cathode is the main determinant of many aspects of battery performance, including energy and power density, calendar and cycle life, and safety. Of the commonly used cathode materials in Li-ion batteries, layered lithium metal oxides ($LiTMO_2$, TM is transition metal) are the most promising candidates for EVs because of their high theoretical capacities (~ 270 mAh/g) and a relatively high average operating voltage (~ 3.6 V vs. Li^+/Li). In the case of $LiCoO_2$, however, only about 140 - 170 mAh/g can be used practically due to a series of irreversible phase transformations occurring at high states-of-charge, and side reactions with electrolytes and other components that are encountered at the high potentials. In addition, the high cost and relative scarcity of Co has driven research focus from $LiCoO_2$ to lower cost alternatives such as

Ni-containing layered oxides. These layered oxides are the focus of this review.

$LiNiO_2$ was first considered as a cathode material because it has the same crystal structure as $LiCoO_2$, and Ni is fairly inexpensive and abundant. Moreover, Ni redox processes occur at a slightly lower potential than Co, allowing for higher accessible capacities in the voltage stability window of the electrolytic solutions.[2, 3] Difficulties in synthesizing high-quality samples of $LiNiO_2$, and concerns with its safety at high states-of-charge led researchers to look for strategies that would lead to more reliable cathode materials. These strategies mainly rely upon substituting other elements for Ni in the layered structure, resulting in a series of Ni-based oxides.[4] For instance, partial substitution of Ni with Co is found to be an effective way to reduce cationic disorder[5] and adding a small amount of Al can improve both thermal and structural stability.[6] Incorporation of Mn is shown to stabilize the layered structure.[7] With this element substitution strategy, several promising compositions, $LiNi_xMn_yCo_zO_2$ (NMC) and $LiNi_{0.8}Co_{0.15}Al_{0.05}O_2$ (NCA), have been identified and have become the most extensively investigated cathode materials. Of these compounds, $LiNi_{0.8}Co_{0.15}Al_{0.05}$ (NCA) can deliver a relatively high capacity of > 180 mAh/g at a moderate voltage and is now used commercially in vehicle battery applications, although there are still concerns about its thermal stability. The most extensively studied NMC composition is $LiNi_{1/3}Mn_{1/3}Co_{1/3}O_2$, also known as NMC-333, which typically delivers a practical capacity of about 160 mAh/g, and exhibits good rate capability.[8] Because the cost and relative scarcity of Co is a concern, compositions with lower Co contents (e.g., NMC-442) have also been investigated extensively. In as-made NMC compounds where the Ni and Mn contents are matched, Ni is generally found to be divalent, Co trivalent, and Mn tetravalent. Only Ni and Co are electroactive, with Mn generally serving as a structure stabilizer.[9, 10] Therefore, to increase specific

[a.] Energy Storage and Distributed Resources Division, Lawrence Berkeley National Laboratory, Berkeley, CA 94720, USA. Email: weitong@lbl.gov
* Corresponding author
‡ Present address: Department of Materials Science and Engineering, Iowa State University, Ames, IA 50011
§ Present address: Department of Chemistry, Virginia Tech, Blacksburg, VA 24061

capacity without adversely impacting cost, it is of interest to increase the Ni content of NMCs, either in matched compositions, or in compositions where the Ni content is higher than Mn (e.g., NMC-532) and is in both the divalent and trivalent states initially. Another possible way to increase specific capacity is to exploit the Ni^{2+}/Ni^{4+} redox couple in Li-rich compounds such as Li_2NiO_2. If it were possible to fully extract both lithium ions in this compound, a high theoretical capacity of 513 mAh/g could be obtained, although structural instabilities (an irreversible phase transformation) prevent good cycling of this material.[11, 12]

Several excellent review articles on rechargeable Li-ion battery cathodes have summarized recent major progress.[1, 2, 13-15] Here, we concentrate on the Ni-based layered oxides, including stoichiometric compounds with one or two lithium ions per formula unit, $LiTMO_2$ and Li_2TMO_2, respectively. The emphasis is on the chemistry of Ni-based layered oxides from the materials design perspective, along with recent advances on the understanding of composition-structure-property relationships. This review is divided into four sections covering the historical development of unsubstituted $LiNiO_2$, $Li_2Ni_{1-x}Tm_xO_2$, Ni-based binary ($LiNi_{1-x}TM_xO_2$), and ternary ($LiNi_{1-x-y}TM_xTM'_yO_2$) systems ($0 < x, y < 1$). In the final sections, exciting new directions involving the possible use of combinatorial approach to rapidly identify promising high-capacity electrode materials, particularly for lithium-excess lithium metal oxide materials are briefly covered.

2. LiNiO₂

Challenges with $LiNiO_2$ can be categorized as follows: (1) synthesis of stoichiometric (or near-stoichiometric) materials, (2) irreversible phase transformations during intercalation/deintercalation, and (3) structural degradation upon exposure to air/moisture and during shelf storage. It is also important to understand the correlation between the synthetic protocols and electrochemical performance to identify the key variables that lead to stoichiometric (or near-stoichiometric) $LiNiO_2$.

$LiNiO_2$ is isostructural with $LiCoO_2$, similar to layered α-$NaFeO_2$ (space group $R\bar{3}m$). In the ideal case (**Figure 1**), nickel and lithium atoms are located in the octahedral *3b* and *3a* sites, respectively, and occupy alternating layers in a cubic close-packed array of oxygen atoms, which occupy the *6c* sites. This type of stacking arrangement
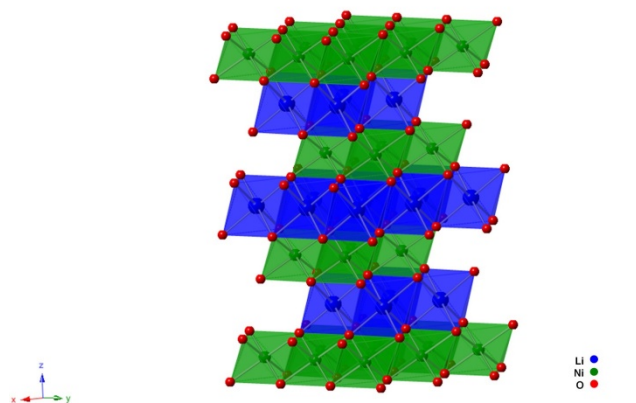
is denoted O3, where O signifies that Li ions are in octahedral sites and the number 3 indicates the number of transition metal slabs per unit cell. This layered structure provides a two-dimensional space for lithium ions to transport, and an ideal stoichiometry should have nickel in the trivalent state. However, it is difficult to synthesize stoichiometric $LiNiO_2$ due to lithium loss and reduction of some Ni^{3+} to Ni^{2+} during thermal calcination, a necessary step in the synthesis. Because of the small differences in the ionic sizes of Ni^{2+} (0.69 Å) and Li^+ (0.76 Å), Ni^{2+} ions can migrate to the octahedral lithium (*3a*) sites, where they may interfere with lithium diffusion. So a more realistic representation of the formula is $Li_{1-z}Ni_{1+z}O_2$. The degree of non-stoichiometry is very sensitive to the synthetic conditions and profoundly affects the electrochemical properties of the final product.[14, 16] Therefore, the synthetic conditions need to be properly controlled in order to produce a high-quality $LiNiO_2$.

A variety of techniques for producing $LiNiO_2$ have been reported in the literature, including solid-state, combustion, sol-gel, microwave-assisted synthesis, Pechini process, chemical vapor deposition, hydrothermal, and ion-exchange methods; see reference 5 for details. This article focuses on $LiNiO_2$ prepared by solid-state[11, 17-28] and combustion methods[29-32] because of their relative popularity and maturity. Both the stoichiometry and electrochemical performance of $LiNiO_2$ are very sensitive to the synthetic conditions (e.g., precursors, annealing atmosphere, etc.). Numerous precursor combinations such as oxides, hydroxides, nitrates, carbonates, and acetates etc. have been employed to produce $LiNiO_2$ under different atmospheres (O_2 and air).[23, 33] The products of several combinations of hydroxides, nitrates, and carbonates as lithium and nickel sources annealed under O_2 delivered a much higher reversible capacity (> 150 mAh/g) in the voltage range of 2.5 to 4.2 V vs. Li^+/Li (0.17 mA/cm^2) compared to the samples annealed under air (**Figure 2**). This better electrochemical activity was ascribed to the more ideal stoichiometry and cation arrangement in the final $LiNiO_2$ products. As reflected by X-ray diffraction studies, the electroactive $LiNiO_2$ samples showed large intensity ratios of (003) to (104) as well as a clear split of the (108) and (110) peaks (**Figure 2**), suggestive of a low number of defects and a high degree of "layeredness".[33] The stoichiometry and degree of ordering in $LiNiO_2$ product is also influenced by the O_2 partial pressure because a sufficient O_2 supply during synthesis helps suppress the reduction of reactive Ni^{3+} and leads to a decrease in the amount of Ni^{2+} in the final product.[34, 35] Studies on the reaction mechanism and kinetics of $LiNiO_2$ formation

Figure 1 Crystal structure of an idealized layered $LiNiO_2$ ($R\bar{3}m$), where lithium, nickel and oxygen are represented by blue, green and red spheres, respectively.
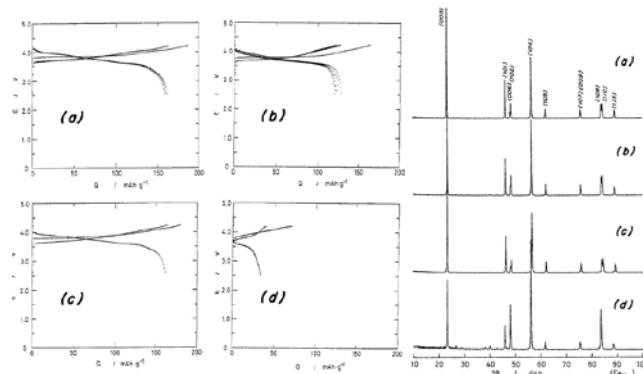

Figure 2 Voltage profiles and x-ray diffraction patterns of $LiNiO_2$ samples showing the effects of precursors and atmosphere: (a) $LiNO_3$+$NiCO_3$, O_2; (b) $LiNO_3$+$NiCO_3$, air; (c) $LiNO_3$+$Ni(OH)_2$, O_2; (d) Li_2CO_3+$NiCO_3$, O_2.[33] Used by permission from reference 33.

also suggested that high O_2 partial pressure (1000 mL/min) is essential to overcome the diffusion barriers of Li and Ni ions in the molten lithium-containing precursor and NiO particles during the solid-state reaction.[26] In addition to the atmosphere, starting precursors also affects the stoichiometry and electrochemical activity of $LiNiO_2$. Reactive precursors that melt and decompose at a low temperature are more favorable than those that are less reactive. Moreover, lithium content in the precursor during synthesis also plays an important role because of the tendency to lose lithium during the calcination process. Arai *et al.* reported the synthesis of $LiNiO_2$ by starting with a 3 molar excess of LiOH precursor to provide sufficient lithium source during reaction and washing the product after calcination to remove residual lithium compounds. The final product exhibited a large reversible capacity of > 200 mAh/g between 3 and 4.5 V vs. Li^+/Li. According to the Rietveld refinement of the x-ray diffraction pattern and chemical analysis, this high capacity was ascribed to the fact that the as-synthesized $LiNiO_2$ was close to stoichiometric. The chemical analysis of $LiNiO_2$ was performed by analyzing the atomic absorption spectroscopy and inductively coupled plasma emission spectroscopy for Li, after dissolving the $LiNiO_2$ sample in hydrochloric acid aqueous solution.[36] Later, $LiNiO_2$ prepared by a combustion method was reported with various excess lithium amounts ranging from 4 to 15%. The sample prepared with 10% excess Li delivered the largest discharge capacity of 195 mAh/g in the voltage range of 2.7 to 4.4 V vs. Li^+/Li at 0.1C.[29] We recently obtained a nearly stoichiometric material with a Li excess as low as 2%, but found that the surface characteristics and electrochemistry of the $LiNiO_2$ product varied depending on the lithium content of the precursor, with the sample made with 10% excess having the best electrochemical properties (200 mAh/g, 2.7 – 4.3 V vs. Li^+/Li, 0.1C).[37] In summary, to obtain a close to ideal stoichiometry of $LiNiO_2$, there are three important factors: (1) reactive precursors (e.g., $LiNiO_3$ and $Ni(OH)_2$) to ensure complete reaction; (2) sufficient O_2 flow to minimize Ni^{2+} formation; (3) excess Li source to compensate for lithium loss during the calcination process. When the synthetic conditions deviate from the optimal, a rock-salt type cubic structure ($Fm\overline{3}m$) can form in the final product , the poor electrical properties of which lead to inferior electrochemical performance (e.g., low capacity, poor rate capability).[25, 33, 38, 39]

The practical specific capacity of $LiNiO_2$ that has been reported in the literature varies with the upper voltage limit, generally increasing with higher cutoffs, but rarely reaches the theoretical value of 274 mAh/g.[30, 33] The material experiences structural transformation during Li deintercalation processes.[17, 33, 36, 40-44] The $LiNiO_2$ phase behavior is typically divided into four regions (**Figure 3**) during deintercalation: original hexagonal phase (H1), monoclinic (M), another hexagonal phase (H2), and, finally a third hexagonal
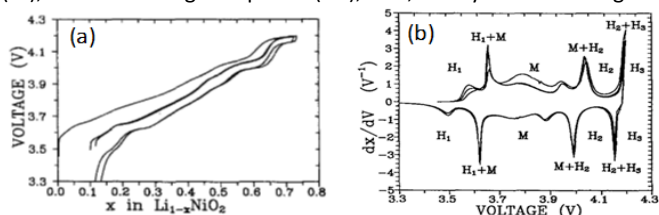
Figure 3 (a) The voltage profiles of $LiNiO_2$ vs. Li cycled at C/100 at 30 °C; (b) The derivative dx/dV, plotted vs. V for the cycles shown in (a).[45] Used with permission from reference 45.
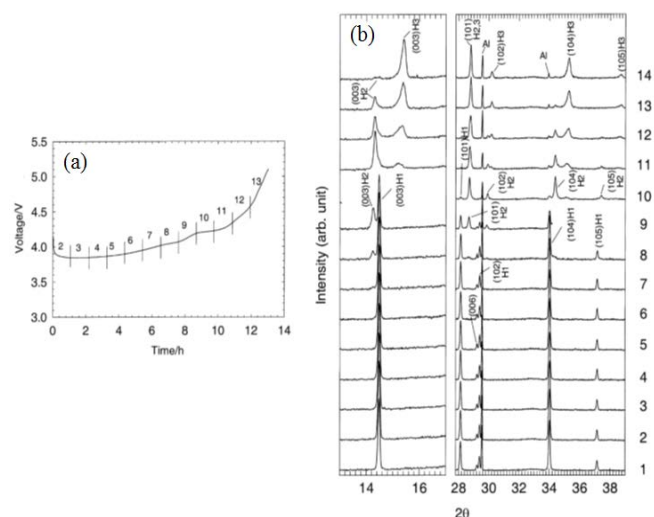
Figure 4 (a) The first charging profile of $Li_{1-x}NiO_2$ at C/13 between 3.0 and 5.1 V, (B) In situ XRD patterns of $Li_{1-x}NiO_2$ in the (003) to (105) region of the hexagonal structure collected at the designated state of charge.[40] Used with permission from reference 40.

phase (H3).[33, 45, 33, 45] In particular, the anisotropic lattice changes along the *a*- and *c*-axes during the H2 and H3 phase transition, resulting in a large volume change (9%), can cause micro-cracks in $LiNiO_2$ particles in electrodes above 4.2 V vs. Li^+/Li (> 0.75 Li deintercalated).[44] In contrast, Yang *et al.* proposed two first-order phase transitions with all phases having a hexagonal structure instead of one having a monoclinic structure based on their *in-situ* synchrotron XRD studies. Possible explanations for this include the source of $LiNiO_2$, likely different degrees of ion mixing, and *in-situ* cell architecture, as evidenced by the differences in cell polarization shown in **Figure 3, 4**.[17, 40, 45] In spite of this discrepancy, the overall diffraction patterns of the three hexagonal phases agreed well (see the example given in **Figure 4**).[40] In addition to XRD characterization, X-ray absorption spectroscopy (XAS) results on electrodes at various states-of-charge are consistent and show: (i) a Jahn-Teller distortion for Ni^{3+}, (ii) electrochemical oxidation of Ni^{3+} to Ni^{4+}, and (iii) an undistorted environment for Ni^{4+}.[21, 46-48] The possible phase changes due to the cooperative Jahn-Teller distortion of Ni^{3+} and high reactivity of Ni^{4+} with electrolyte are believed to be responsible for the capacity decay that is generally observed.

In addition to the capacity fading associated with phase transformations at high states-of-charge, the sensitivity of $LiNiO_2$ to air and moisture exposure is also a challenge. The electrochemical performance of $LiNiO_2$ degrades after storage in air for a period of time. The performance decay is related to the chemical instability of $LiNiO_2$ in air. During storage, the spontaneous reduction of Ni^{3+} to Ni^{2+} occurs, resulting in a loss in structural ordering. Moreover, active oxygen species (O^-, O_2^-) form on the surface and leads to the production of Li_2CO_3 in the presence of CO_2.[49] The difficulties in controlling synthesis and the intrinsic instability of unsubstituted $LiNiO_2$ during cycling led researchers to try elemental substitution to improve performance.

3. $Li_2Ni_{1-x}TM_xO_2$

Within the Li-Ni-O chemical space, Li_2NiO_2 also has aroused interest because of the very high theoretical capacity of 513 mAh/g based on
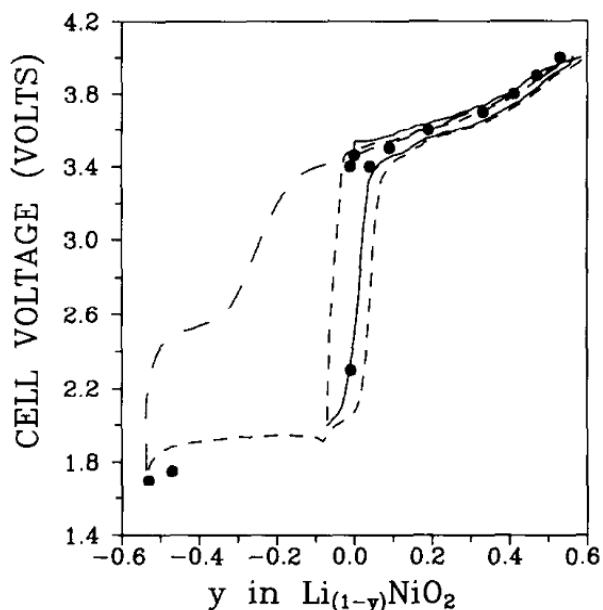
Figure 5 Three cycles of a cell containing LiNiO₂ initially discharged to form 1T-Li₂NiO₂: (solid) first charge and discharge to 2.0 V; (small dashed) second charge and discharge to 1.7 V; (large dashed) third charge.[11] Used with permission from reference 11.

full utilization of the Ni^{2+}/Ni^{4+} redox couple and extraction of two lithium ions per formula unit. The first electrochemical study of Li_2NiO_2 was carried out by Dahn and coworkers in 1990, who prepared it by intercalating one extra Li into layered $LiNiO_2$. **Figure 5** shows the voltage profiles of $Li_{(1-y)}NiO_2$ discharged to different lower potential limits.[11] A plateau around 1.9 V associated with the insertion of a second Li can be clearly observed. The Li_2NiO_2 formed by the electrochemical lithiation method is isostructural with $Ni(OH)_2$ and has the $1T$-TiS_2 structure, therefore, is denoted $1T$-Li_2NiO_2. The structure ($P\overline{3}m1$ space group) consists of hexagonally close-packed layers of oxygen with Ni filled octahedra and Li filled tetrahedra (**Figure 6**). This additional Li can be removed from Li_2NiO_2 during the subsequent charge and the host lattice reverts to the original $LiNiO_2$ structure, but there is substantial hysteresis in the voltage profiles because of the large electrostatic repulsion between tetrahedral Li ions.[11]

The $1T$-Li_2NiO_2 phase can also be prepared by chemically lithiating layered $LiNiO_2$ using lithium benzophenone.[11] It cannot be prepared directly by high-temperature synthesis, because the
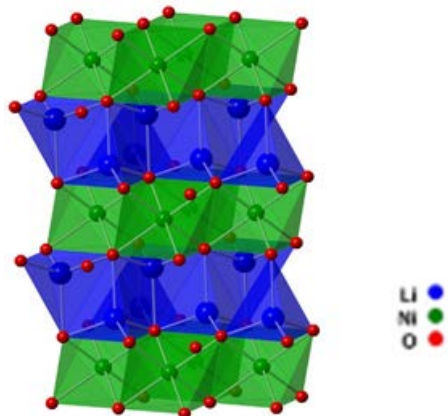

Figure 6 Crystal structure of $1T$ - Li_2NiO_2, $P\overline{3}m1$ space group. Li, Ni, and O ions are indicated by blue, green, and red spheres, respectively.
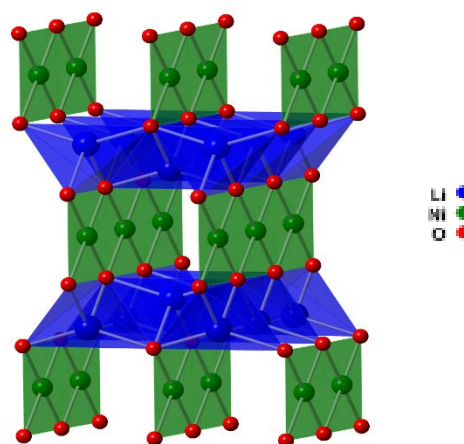

Figure 7 Crystal structure of Li_2NiO_2, *Immm* space group. Li, Ni, and O ions are indicated by blue, green, and red spheres, respectively.

ground state of Li_2NiO_2 is not the 1T-structure, but an orthorhombic form (*Immm* space group). The $1T$-Li_2NiO_2 phase converts to the orthorhombic structure at 400 ⁰C.[28] In the *Immm* structure, Ni sits at the center of an oxygen rectangle and Li occupies tetrahedral sites (**Figure 7**). First-principles calculations predict a reasonably good ionic conductivity for orthorhombic Li_2NiO_2 due to the two-dimensional Li diffusion along the *b* axis and in the diagonal direction between the *a* and *b* axes in the structure.[50] It is possible to prepare orthorhombic Li_2NiO_2 by solid-state synthesis; e.g., by annealing Li_2O and NiO precursors at 650 ⁰C for 24h under inert atmosphere to prevent oxidation of Ni^{2+} during synthesis.[12, 51] The as-prepared orthorhombic Li_2NiO_2 exhibits a high initial charge capacity (~ 320 mAh/g) but a discharge capacity of only about ~ 240 mAh/g in a voltage range of 1.5 - 4.6 V vs. Li^+/Li (**Figure 8**).[12] There is a large hysteresis between the first charge and the subsequent discharge, which resembles that of lithiated $1T$-Li_2NiO_2 with plateaus around 3.7 and 1.9 V. Using *ex situ* XRD and EXAFS techniques, it was found that the orthorhombic *Immm* structure gradually transformed to the layered structure during the 1ˢᵗ cycle and eventually became amorphous after cycling.[12]

To address the structural instability, solid solutions of isostructural Li_2CuO_2 and Li_2NiO_2 have been prepared and studied. The intermediate composition, $Li_2Cu_{0.5}Ni_{0.5}O_2$, exhibited a high reversible capacity of 250 mAh/g that was retained after 15 cycles (1.5 - 4.0 V vs. Li^+/Li, 0.6 mA /cm²).[52] However, there is no direct evidence that Cu can stabilize the structure. The electrochemical
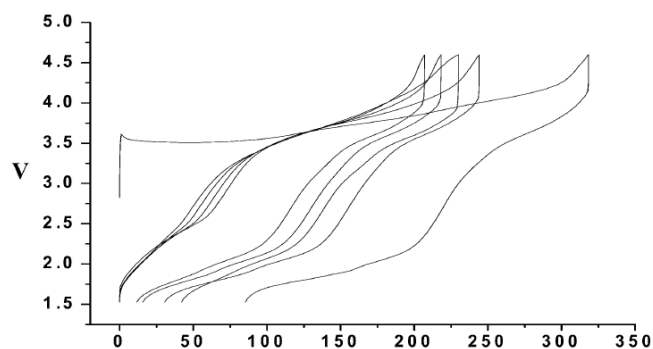

Figure 8 Voltage profiles of a Li half cell containing orthorhombic Li_2NiO_2 cycled in the voltage range 1.5 – 4.6 V at a current density of 12.5 mA/g.[12] Used with permission from reference 12.
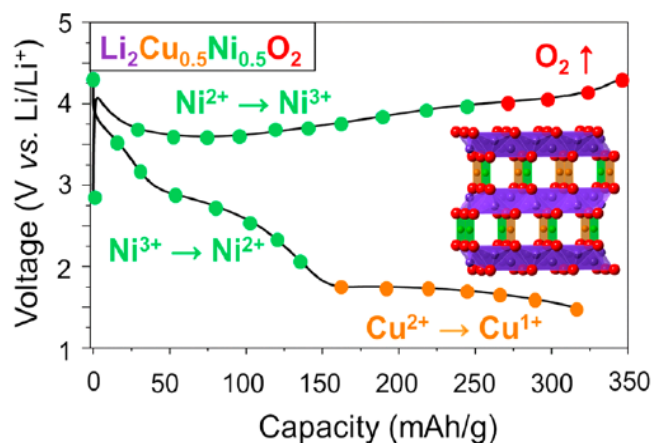
Figure 9 First-cycle voltage profiles of $Li_2Cu_{0.5}Ni_{0.5}O_2$ between 4.3 and 1.5 V at a current density of ~ 70 mA/g along with the proposed electrochemical reaction mechanism.[53] Used with permission from reference 53.

reaction mechanism of $Li_2Cu_{0.5}Ni_{0.5}O_2$ was recently studied using a combination of XAS, and gas evolution measurements, showing that oxidation of Ni^{2+} to Ni^{3+} coupled with O_2 evolution occurs at high potentials (> 3.9 V). The reverse reaction only contributes 125 mAh/g to the discharge capacity, with the rest due to Cu^{2+} to Cu^+ reduction at potentials below 1.8 V (**Figure 9**).[53] No element has been demonstrated so far that can stabilize the planar 4-fold coordination of Ni^{3+} upon Li removal in the *Immm* structure, making the use of this material as a cathode very challenging.[12] Instead, the facile decomposition of this compound at charging potentials of common electrodes (e.g. 4 V for $LiCoO_2$) and the large first charge capacity (> 300 mAh/g) make it suitable as a source of extra lithium to compensate for the Li loss on the negative electrode.[51, 54, 55] For example, $LiCoO_2$ mixed with 4 wt% Li_2NiO_2 additive enabled 100% reversible capacity in a $LiCoO_2$/graphite full cell with no negative impact on the performance, showing that it could be used to balance a cell in which first cycle inefficiencies occur.[51]
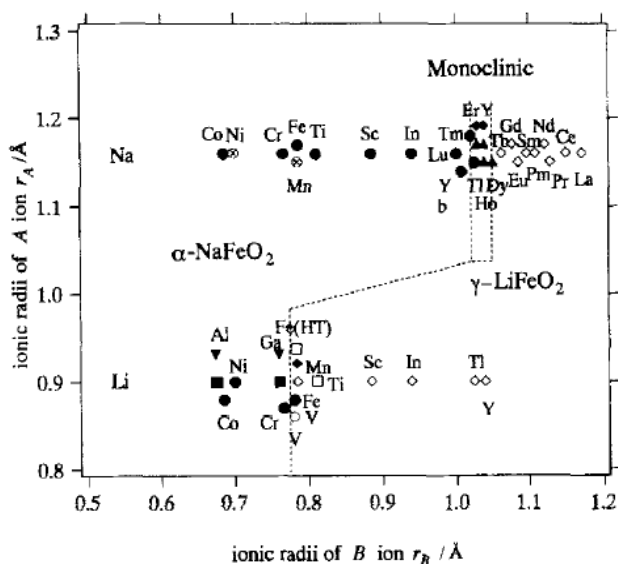

Figure 10 Structure field map for AMO_2 compounds: (●) α-$NaFeO_2$ (rhombohedral); (▼) high-pressure phase; (⊗) α-$NaFeO_2$ (monoclinic); (○) high-pressure phase; (■) Wurtzite ($LiGaO_2$), β-GeO_2; (□) NaCl (disorder); (▲) monoclinic; (◇) $LiFeO_2$ (tetragonal); (◆) orthorhombic (corrugated layer); and HT: high-temperature phase.[56] Used with permission from reference 56.

4. Binary $LiNi_{1-x}TM_xO_2$ (0 ≤ x ≤ 1)

As described in the previous section, $LiNiO_2$ undergoes a series of phase transitions as lithium is extracted from the lattice. A strategy of partial substitution with various elements has been widely employed in order to stabilize the crystal structure. These substituting elements usually impose effects on the "layeredness" and phase stability upon lithium removal, which in turn affect the electrochemical performance, e.g., capacity, rate capability, thermal stability, and cycle life. The thermodynamically stable ordering between lithium and transition metal cations largely depends on the size of the cation. In the case of lithium metal oxides, $LiTMO_2$ (TM = V, Cr, Co, and Ni), are observed to form layered structures, while those with Ti, Mn, and Fe, which have larger ionic radii, form a disordered rock salt or a tetragonally ordered structure. **Figure 10** shows the structure field map for AMO_2 compounds, which provides guidance for the search of new materials having similar structure to $LiNiO_2$.[56]

4.1 $LiNi_{1-x}Co_xO_2$ (0 ≤ x ≤ 1)

Co was used as one of the first cationic substitutions for Ni, as demonstrated by Delmas *et al.* in the early 1990s.[57] A solid solution can form within the whole composition range of $LiNi_{1-x}Co_xO_2$ (0 ≤ x ≤1) system, with Ni^{3+} and Co^{3+} homogeneously located at octahedral transition metal (*3b*) sites in the cubic-close packed oxygen array.[27, 58, 59] The mixed metal system potentially offers cost or performance benefits compared to its end members, $LiCoO_2$ and $LiNiO_2$, respectively. At Co contents below x = 0.5, voltage profiles are very similar to $LiNiO_2$, while, in the Co-rich region, the charge profiles show two plateaus; an initial low V plateau at potentials close to those observed for $LiNiO_2$ followed by a high V plateau close to those of $LiCoO_2$ (**Figure 11**).[57] Moreover, Co substitution substantially stabilizes the crystal structure and improves the Li stoichiometry, making the synthesis less sensitive to experimental conditions. For example, with 20% Co substitution, a nearly stoichiometric oxide can be synthesized in air.[60, 61] The structural stabilization can be more precisely described as improvement in layered characteristics because substitution of smaller Co ions results in lattice contraction and suppresses the migration of Ni to the Li sites,[62-64] which is an important determinant of electrochemical performance (reversible capacity and cycle life).[35] The evolution of electronic structure associated with Ni oxidation from Ni^{3+} to Ni^{4+} has been clearly observed by *in situ* hard XAS studies during charge, whereas the Co oxidation state change is either none or a small amount towards the end of charge.[58, 65] Composition studies over the whole range (0 ≤ x ≤ 1 in $LiNi_{1-x}Co_xO_2$) show that the optimal Co content is around 0.2 to 0.3. For the x = 0.2 composition, the initial capacity is as high as about
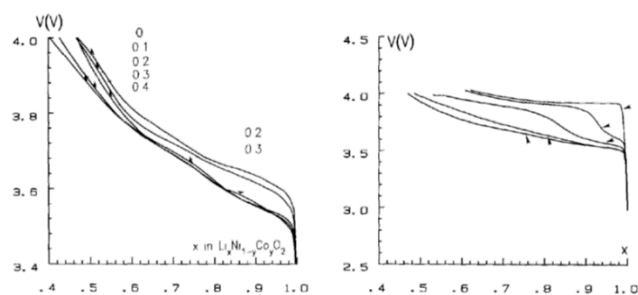

Figure 11 Charge profiles of a $Li//Li_xNi_{1-y}Co_yO_2$ at various Co contents (y).[57] Used with permission from reference 57.
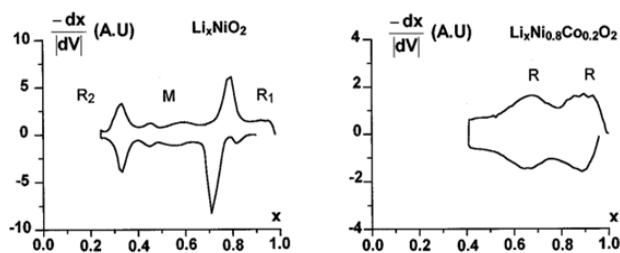
Figure 12 Comparison of the derivative curves for Li_xNiO_2 and $Li_xNi_{0.8}Co_{0.2}O_2$.[73] Used by with permission from reference 73.

Figure 14 The discharge profiles of ion-exchange (IE) and solid state (SS) $LiNi_{0.5}Mn_{0.5}O_2$ at various rates. The cells were charged to 4.6 V at C/20 and kept for 5 hours. 1C corresponds to 280 mAh/g.[7] Used with permission from reference 7.

190 mAh/g when cycled below 4.5 V.[57, 66-69] Due to the improved characteristics of $LiNi_{0.8}Co_{0.2}O_2$, including high capacity, improved structural and thermal stability, as well as lower cost compared to $LiCoO_2$, it was quickly recognized to be preferable to $LiNiO_2$.[68, 70-72]

Sharp oxidation/reduction peaks in the dq/dV plots of $LiNiO_2$ cells are correlated with the phase transformations observed in the x-ray diffraction data during the 1st charge process. In contrast, no obvious oxidation peaks were observed in the dq/dV plots of $LiNi_{0.8}Co_{0.2}O_2$ cells (**Figure 12**) until > 0.6 Li was extracted, indicating that the presence of Co within the transition metal layers prevented the H1 to M phase transformation that occurs below removal of 0.5 Li.[73] This was consistent with crystal structure evolution studies on chemically delithiated samples, which showed the initial structure remained and no oxygen was lost upon extraction of 0.7 Li per formula unit. Furthermore, improved thermal stability of electrochemically delithiated $LiNi_{0.8}Co_{0.2}O_2$ compared to $LiNiO_2$ was observed in differential scanning calorimetry (DSC) measurements (**Figure 13**), although, in both cases, heat flow increased when electrodes were charged to a higher potential.[69] The improved stability has been attributed to the differences in electronic structure of Co^{3+} ($3d^6$ ($t_{2g}^6e_g^0$)) and Ni^{3+} ($3d^7$ ($t_{2g}^6e_g^1$)).[74-76] However, it is full of contradictions; the Co-substituted material shows better thermal stability when delithiated, but the electronic argument implies that oxygen loss will occur more readily. Further understanding of the oxygen behavior and how it relates to thermal stability is clearly needed.

The electrochemical performance of $LiNi_{1-x}Co_xO_2$ compounds is strongly related to the number of structural defects, crystallinity, morphology, and particle size.[67, 72, 77, 78] For Ni-rich compositions (x ≤ 0.2), the presence of extra Ni ions in the inter-slab space becomes more likely, with this tendency becoming more severe if the lithium content is deficient.[79] Furthermore, to prevent formation of NiO, the annealing temperature should not exceed 900 °C.[68]

4.2 $LiNi_{1-x}Mn_xO_2$ (0 < x < 1)

The $LiNi_{1-x}Mn_xO_2$ (0 ≤ x ≤ 1) phase system was initially studied by Dahn's group who reported that solid solutions with the α-NaFeO₂
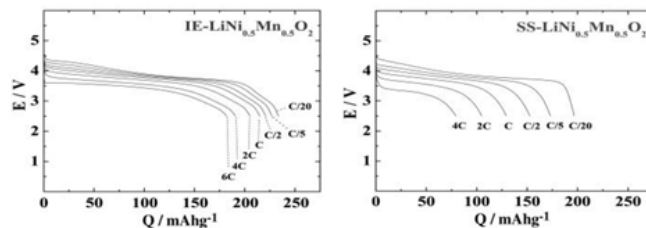
layered structure formed for x ≤ 0.5. The observed capacity decrease as Mn content rose was attributed to the combined effects of cation mixing and the presence of inert Mn^{4+}.[80] For this series of compounds, $LiNi_{0.5}Mn_{0.5}O_2$ became the most widely studied composition after the pioneering work performed by Ohzuku *et al.*, who first reported a high reversible capacity of 200 mAh/g in lithium half cells (2.5 - 4.5 V, 0.17 mA/cm²). Their cathode material was synthesized by annealing a mixture of LiOH and $Ni_{0.5}Mn_{0.5}(OH)_2$ at 1000 °C in air[81, 82]. Other advantages of $LiNi_{0.5}Mn_{0.5}O_2$ compared to $LiNiO_2$ include a lower degree of thermal runaway, and mitigated side reactions with electrolytes in the charged state.[83, 84, 85]

For the $LiNi_{1-x}Mn_xO_2$ (0 ≤ x ≤ 1) system, lithium deficiencies with compensating Ni^{2+} ions on *3a* sites do not occur, instead, there is true anti-site mixing, with Li ions on nickel sites and *vice versa*.[1, 86] Regardless of how it is synthesized, around 10% of the Ni is present on the Li sites.[87, 88] The anti-site defects impede the kinetics of Li diffusion similar to that seen with the defects in $LiNiO_2$.[83, 89, 90] A high reversible capacity (200 mAh/g) of $LiNi_{0.5}Mn_{0.5}O_2$ can only be achieved at low current densities (2.5 - 4.5 V vs. Li^+/Li, 0.17 mA/cm²).[82] To solve this problem, Kang *et al.* prepared a high rate-capability $LiNi_{0.5}Mn_{0.5}O_2$ compound (**Figure 14**) *via* ion exchange from its sodium counterpart, $NaMn_{0.5}Ni_{0.5}O_2$, which has nearly perfect ordering. The amount of cation mixing in the ion-exchanged material decreased to 4.3% based on the XRD refinement. The soft chemical approach was performed at a relatively low temperature so that only Na ions were replaced by Li ions, keeping the rest of the structure intact.[7] The exchange conditions determine the defect chemistry of $LiNi_{0.5}Mn_{0.5}O_2$ and are difficult to control.[91]

The defect chemistry of $LiNi_{1-x}Mn_xO_2$ (0 ≤ x ≤ 0.5) solid solutions varies with composition. The anti-site mixing between Li^+ and Ni^{2+}
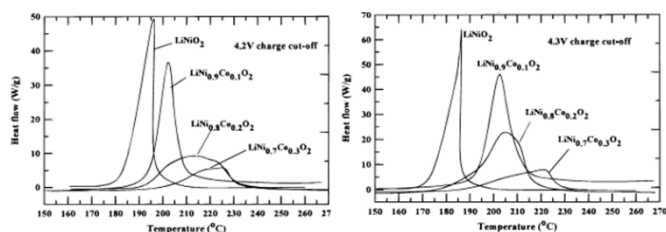

Figure 13 DSC curves of $LiNi_{1-x}Co_xO_2$ electrodes containing electrolyte for x = 0, 0.1, 0.2, and 0.3 after charging them at 4.2 and 4.3 V.[69] Used with permission from reference 69.
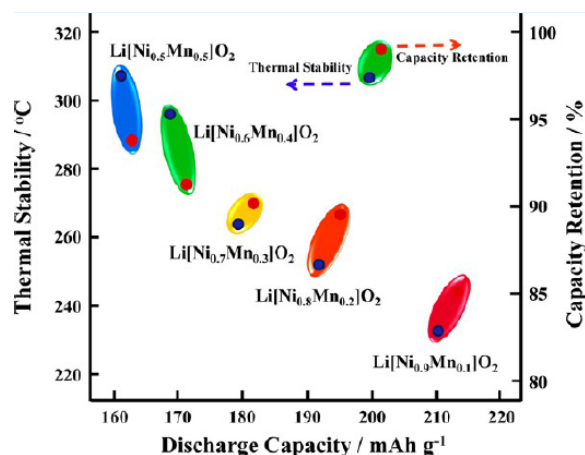

Figure 15 Electrochemical performance of $LiNi_{1-x}Mn_xO_2$ (0.1 ≤ x ≤ 0.5) as a function of composition.[93] Used with permission from reference 93.

ions decreases from 10% to about 3% as x (Mn content) is reduced from 0.5 to 0.1.[92, 93] In Ni-rich compositions, some Ni is present as Ni^{3+} while Mn is in the tetravalent state.[92] From the structural perspective, Mn^{4+} ions are more desirable in terms of circumventing the Jahn-Teller distortion related to Ni^{3+}, which can de-stabilize the de-intercalated material.[87] The combined impact of composition on the electrochemical properties of $LiNi_{1-x}Mn_xO_2$ ($0.1 \leq x \leq 0.5$) can be summarized as follows: the higher the Mn content, the lower the discharge capacity but the better the capacity retention and thermal stability (**Figure 15**).[93]

In addition to O3 layered structures, an O2-type layered phase, $Li_{2/3}Ni_{1/3}Mn_{2/3}O_2$ prepared by ion exchanging Na for Li from the corresponding sodium bronze, $Na_{2/3}Ni_{1/3}Mn_{2/3}O_2$, has been reported. In O2-type structures (**Figure 16**), Li^+ is located in octahedral sites (O) and the unit cell consists of two layers of MO_2 sheets (M = Ni, Mn); they do not have cubic close packed oxygen lattices. This different stacking arrangement of the transition metal layers prevents conversion to spinel upon electrochemical cycling, a common problem with the O3 layered oxides containing redox active Mn^{3+}, which shares in common with the spinel structure a cubic close-packed array of oxygen ions. However, $O2-Li_{2/3}Ni_{1/3}Mn_{2/3}O_2$, is not likely to be used as the sole cathode in lithium-ion batteries as only about half of its total reversible capacity can be extracted and direct synthesis of this phase has proven to be difficult.[94-97]

4.3 LiNi$_{1-x}$Al$_x$O$_2$ (0 < x < 1)

Al was investigated as a non-transition metal substituting element for several reasons. First of all, α-$LiAlO_2$ is isostructural with $LiNiO_2$. Second, according to first-principles calculations, Al substitution for transition metals in $LiTMO_2$ should lead to higher Li intercalation
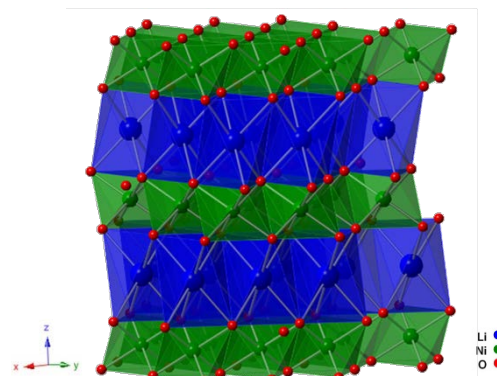

Figure 16 Crystal structure of layered O_2 structure, where lithium, nickel and oxygen are represented by blue, green and red spheres, respectively.

potentials due to the participation of oxygen in electron exchange that is driven by the fixed valence state of Al.[98, 99] Third, Al substitution may stabilize the crystal structure of $LiTMO_2$ as demonstrated by the ability to prepare $O3-LiMn_{1-y}Al_yO_2$ directly, unlike other O3 Mn-containing compounds.[100] Finally, Al is of interest as a constituent in the $LiTMO_2$ compound due to its low cost and light weight.[101]

The enthalpy of Al-substitution in lithium nickel oxide is positive, indicating a tendency for phase separation. Layered $LiNi_{1-x}Al_xO_2$ solid solutions can only form at high temperatures where the entropy contribution surpasses the positive enthalpy and leads to a negative Gibbs free energy.[102] Independent of the synthetic methods used, pure layered $LiNi_{1-x}Al_xO_2$ solid solutions form in a concentration range of $0 \leq x \leq 0.5$.[103, 104] Substitution with Al can stabilize Ni^{3+} and maintain the two-dimensionality of the crystal lattice in the layered structure.[101, 104, 105] However, Al^{3+} substitution has a limited effect in reducing Li^+/Ni^{2+} cation

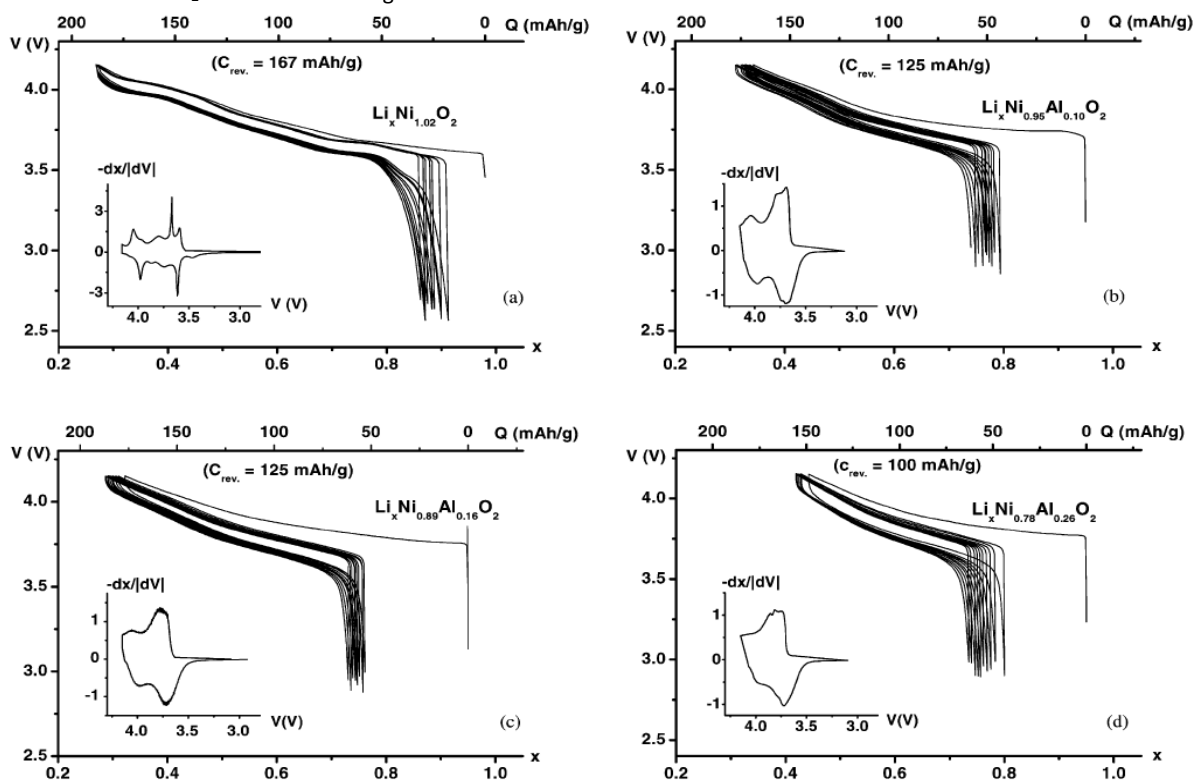**Figure 17** Variation of the cell voltages vs. Li content for the first 10 cycles of $Li_xNi_{1-y}Al_yO_2$ at C/20. (a) y = 0, (b) y = 0.10, (c) y = 0.15, and (d) y = 0.25.[103] Used with permission from reference 103.

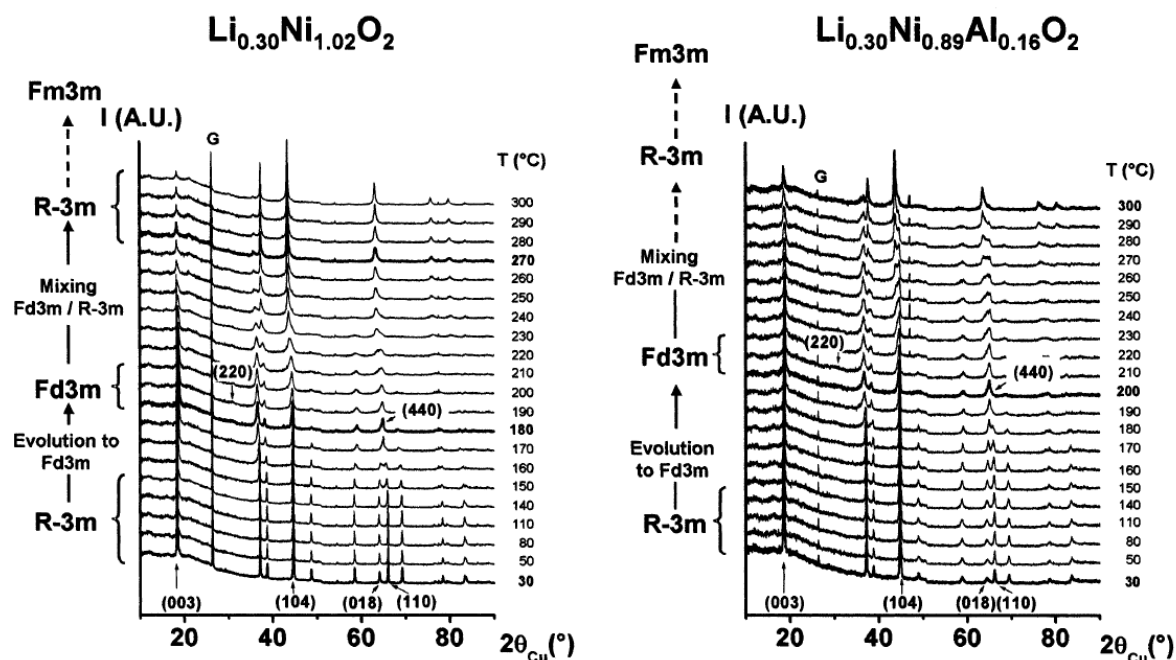**Figure 18** In-situ XRD patterns of $Li_{0.3}Ni_{1.02}O_2$ and $Li_{0.3}Ni_{0.89}Al_{0.16}O_2$ upon increasing temperature (XRD data were collected for 1h after 10 min once samples were heated to each temperature at a heating rate of 15 $^{\circ}$C/min).[41] Used with permission from reference 41.

mixing. About 5% extra Ni^{2+} is present on the Li sites for $LiNi_{1-x}Al_xO_2$ (x = 0.1 − 0.5),[103] but the amount is very sensitive to synthetic conditions (e.g., the presence of Ni^{2+} on Li sites in $LiNi_{0.75}Al_{0.25}O_2$ can be minimized to as low as 0.6% by using a strongly oxidizing Li_2O_2 precursor).[106] On the nanometer-scale, a tendency for Ni^{3+} and Al^{3+} to segregate on the (11l) planes rises with increasing Al concentration, due to the differences in electronegativity of Al^{3+} and Ni^{3+} ($\chi(Al^{3+})$ = 1.61 and $\chi(Ni^{3+})$ = 1.91).[107] The most notable effects of Al substitution on electrochemical performance are the dramatic improvement in cycle life and safety at the expense of reversible capacity.[41, 103, 108-111] For instance, the reversible capacity decreases from 167 mAh/g (x = 0) to 100 mAh/g (x = 0.25) when cycling $LiNi_{1-x}Al_xO_2$ in lithium half cells between 3 and 4.15 V (**Figure 17**).[103] For this reason, most studies on the electrochemistry of $LiNi_{1-x}Al_xO_2$ focused on compositions with x < 0.3. The negative effect on reversible capacity is attributed to the electrochemically inactive character of Al within the voltage window of interest.

Al substitution also prevents cell over-charging and avoids phase transformation during Li deintercalation. 10% Al is sufficient to suppress the phase transformations observed in the $LiNiO_2$ system and leads to optimal performance in terms of reversible capacity and cyclability.[103] Another pronounced effect of Al substitution is thermal stabilization.[41, 110, 111] Heating the charged $Li_yNi_{1-x}Al_xO_2$ electrodes leads to a series of phase transformations from layered $R\overline{3}m$ to spinel $Fd\overline{3}m$, and eventually to cubic $Fm\overline{3}m$ (**Figure 18**), where the initial transformation to $Fd3m$ is achieved through the migration of Ni and Al cations from slab to the inter slab space and the displacement of Li ions from octahedral to tetrahedral sites in the inter slab space. The stability of Al^{3+} in the tetrahedral environment is believed to disrupt the cation migration that is necessary for the phase transformation, thereby, slowing down the phase transformation kinetics and leading to more thermally robust features.[41]

4.4 $LiNi_{1-x}Fe_xO_2$ (0 < x < 1)

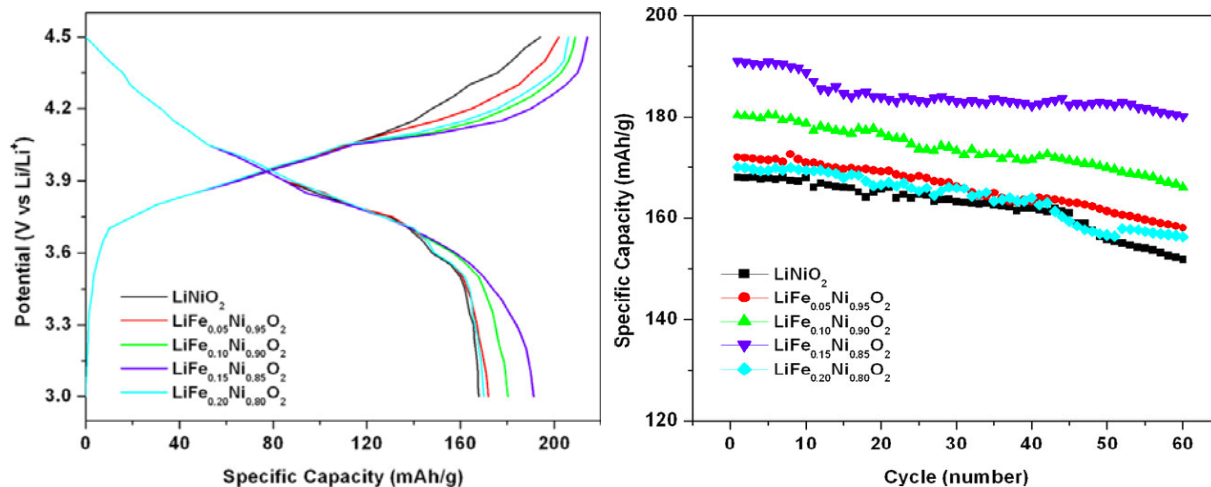**Figure 19** Voltage profiles and cycling performance of $LiNi_{1-x}Fe_xO_2$ (0 ≤ x ≤ 0.2) cathodes at 0.5C between 4.5 and 3 V.[118] Used with permission from reference 118.

The low cost and toxicity of Fe make it attractive as a substituent, but the effect is quite different from that of Co and Mn. A number of polymorphs of $LiFeO_2$ exist, including the disordered rock salt α-$LiFeO_2$ ($Fm\overline{3}m$), tetragonal γ-$LiFeO_2$ ($I4_1/amd$), and β-$LiFeO_2$ with intermediate ordering ($C2/c$). Although the crystal structure depends largely on the synthetic route, γ-$LiFeO_2$ cation ordering is electrostatically favored and typically obtained because the size difference between Li^+ and Fe^{3+} is small.[112] In the $LiNi_{1-x}Fe_xO_2$ ($0 \leq x \leq 1$) system, layered structures are only obtained for $x < 0.3$ during solid state preparation; further increasing the Fe content leads to a cubic rock-salt phase due to the occupancy of Fe in the Li layers.[113, 114] Even for samples prepared by ion exchange of α-$NaNi_{1-x}Fe_xO_2$ in LiCl/KCl molten salts at 400 °C, significant cation disordering was still detected in the Fe-rich region ($x = 0 - 0.5$) and attempts to extract Li during the 1st charge were not successful.[56] Within the solid solution composition range, the $LiNi_{1-x}Fe_xO_2$ system shows similar defect chemistry as lithium nickel oxide; some Fe and Ni ions replace Li on Li sites leading to a general formula, $Li_{1-z}(Ni_{1-x}Fe_x)_{1+z}O_2$, when $0 \leq x \leq 0.3$.[113, 115-117] The best electrochemical performance in the $LiNi_{1-x}Fe_xO_2$ ($0 \leq x \leq 1$) system was reported on $LiFe_{0.15}Ni_{0.85}O_2$ made by a sol-gel method from an aqueous solution of metal nitrate precursors heated to 600 °C for 10 h under O_2 flow. The as-synthesized sample delivered a high reversible capacity of 191 mAh/g (3 - 4.5 V vs. Li^+/Li, 0.5C), with 94% capacity retention after 60 cycles (**Figure 19**). This relatively good performance was generally ascribed to the high degree of layeredness, crystallinity, uniform morphology, and narrow particle size distribution of the material.[118]

4.5 $LiNi_{1-x}Fe_xO_2$ ($0 < x < 1$)

Ti substitutes as a tetravalent ion analogous to Mn^{4+} in $Li(Ni^{2+}_{0.5}Mn^{4+}_{0.5})O_2$. Because Ti^{4+} substitution increases the amount of Ni^{2+} in the transition metal layers, it was originally thought that it could prevent its migration to the Li layers. While all $LiNi_{i-x}Ti_xO_2$ samples retain a layered $R\overline{3}m$ structure when $x \leq 0.3$,[119, 120] cation mixing was not alleviated; in fact, it increased with Ti content.[120, 121] Both Ni^{2+} (0.83 Å) and Ti^{4+} (0.745 Å) have a relatively large ionic size that make them tend to migrate to the Li layer.[122] The presence of many of these defects results in poor electrochemical performance; for example, $LiNi_{0.7}Ti_{0.3}O_2$ sample annealed in air only delivered a discharge capacity of < 30 mAh/g.[120, 123] Reasonably good capacity (> 150 mAh/g) is
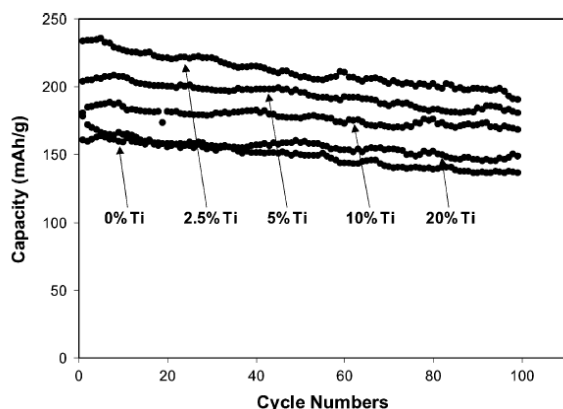
typically achieved only when the Ti content is below $x = 0.1$.[124-129] In this substitution range, $LiNi_{0.975}Ti_{0.025}O_2$ delivered the largest discharge capacity (235 mAh/g, 2.8 - 4.3 V vs. Li^+/Li, 0.2 mA/cm^2), but further increasing the Ti content led to a reduced reversible capacity (**Figure 20**). These observations can be explained by the relative amounts of anti-site defects and the electrochemical inactivity of Ti^{4+} in the tested voltage range.[125, 126] Both X-ray and neutron diffraction studies suggested the amount of TM on Li sites increases with Ti content, so that the significant decrease of the capacity with higher Ti concentration can be directly attributed to the higher degree of cation mixing induced by Ti substitution.[121]

4.6 Other Substitutions

Substitution of Ni^{3+} with Ga^{3+}, which is similar in size (Ni^{3+} (radius 0.74 Å) and Ga^{3+} (radius 0.76 Å)) has been proposed to prevent valence fluctuation and Li-ion rearrangement, resulting in a uniform Li-ion distribution at a high state-of-charge and thereby prohibiting phase separation. $LiNi_{0.98}Ga_{0.02}O_2$ prepared by firing lithium nitrate, gallium nitrate, and nickel carbonate precursors at 660 °C under O_2 delivered a superior rechargeable capacity of 190 mAh/g and good retention of > 95% after 100 cycles between 3.0 and 4.3 V (**Figure 21**). Based on the shapes of the pseudo-OCV charge curves, it appears that a single hexagonal structure was retained throughout the charge process without formation of a monoclinic phase or two-hexagonal-phase region for this electrode.[130]

Substitution with Sb^{5+} was motivated by the electrochemical properties of $Li(Ni^{2+}_{0.5}Mn^{4+}_{0.5})O_2$, in which Ni^{2+} participates in the redox reaction and Mn^{4+} functions as structural stabilizer. The incorporation of cations with high valence states results in increased amounts of Ni^{2+} in the structure, compared to the unsubstituted parent compound. Substituting Sb^{5+} increases the Ni^{2+} content by 67% for the end-member composition $Li(Ni^{2+}_{2/3}Sb^{5+}_{1/3})O_2$. Only the Ni is redox active and with the increased Ni^{2+} content, there is less of a tendency to form Ni^{4+} at high states-of-charge, which reduces electronic conductivity and can result in deleterious side reactions with electrolytic solutions. Attempts to synthesize $LiNi_{2/3}Sb_{1/3}O_2$ by solid-state reactions led to the formation of an orthorhombic phase in the $Fddd$ space group. Layered $LiNi_{2/3}Sb_{1/3}O_2$ with $R\overline{3}m$ structure could only be prepared by ion-exchange of $NaNi_{2/3}Sb_{1/3}O_2$, but the product only delivered an initial discharge capacity of 92 mAh/g (2.5 - 4.6 V vs. Li^+/Li) and suffered a fast capacity fade. The low capacity

Figure 20 Cycling performance of $LiNi_{1-x}Ti_xO_2$ ($0.025 \leq x \leq 0.2$) samples at a current density of 0.2 mA/cm^2.[126] Used with permission from reference 126.
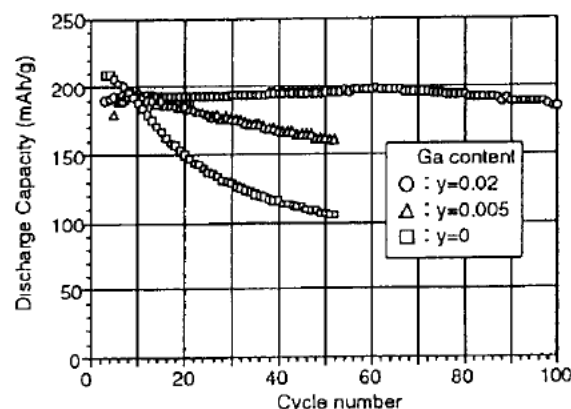

Figure 21 Cycling plots of gallium-substituted $LiNiO_2$ (4.3 - 3 V, 36 mA/g).[130] Used with permission from reference 130.

was attributed to Ni^{2+} migration to Li sites (Li/Ni intermixing increase from 0.2% to ~ 10.4% after five cycles) during cycling. The driving force is provided by strong electrostatic repulsion as each Ni ion is surrounded by three Sb^{5+} and three Ni^{3+} when $LiNi_{2/3}Sb_{1/3}O_2$ is partially charged.[131]

The substitution of other elements such as Mg, B[132, 133], Cu[126], and F[134, 135] into $LiNiO_2$ has also been attempted. A small amount of Mg^{2+} or Cu^{2+} ions may replace the Ni^{2+} ions that are often located in *3a* sites in the as-prepared lithium nickel oxide. Another hypothesis was the electrochemical inactivity of these divalent cations prevents full oxidation to Ni^{4+}, retaining more Li in the structure and moderating the *c* lattice parameter change in the deeply charged state. The presence of electronegative fluorine in the oxygen lattice is also expected to change the chemical environment of Ni. For all of these elements, the studied substitution levels were low (< 0.2) and solid solutions formed in most cases. For instance, no secondary phase was observed for Mg or F substitution at a concentration between 0 and 0.2.[133, 135] In contrast, B substitution resulted in residual glass-like impurities.[132] In most cases, substitution resulted in lower capacity and no clear evidence of improvement in electrochemical performance over unsubstituted $LiNiO_2$ was shown. In contrast to the negative effect of immobile cations on the Li sites, Mg^{2+} substitution below 0.02 improved the cycling stability, because the presence of Mg^{2+}, which is similar in size to Li^+, in the inter-slab space, prevents local structural collapse.[133] This indicates a small amount of redox inactive and immobile cations may be good for structural stabilization, but a large amount is not because it slows the Li diffusion. Improvements in the cycling performance of a material in which 0.015 F was substituted on oxygen sites was ascribed to the partial suppression of the undesired phase transitions during charge/discharge processes.[134]

5 $LiNi_{1-x-y}TM_xTM'_yO_2$ (0 < x, y < 1)

The most technologically important Ni-containing layered oxides for Li-ion batteries are based on Ni-Mn-Co (NMC) and Ni-Co-Al (NCA) metal combinations. There is a large pool of literature on NMC compounds; see several excellent cathode review articles.[1, 14, 136, 137] Most of these reviews focus on compositions with Ni content below 0.5. Recently, there has been a trend towards increasing the Ni content in stoichiometric layered metal oxides (one Li per transition metal) to increase the practical energy density. Here we focus on $LiNi_{1-x-y}Mn_xCo_yO_2$ (0 < x, y < 1) compositions with a much wider Ni range (1-x-y from 1/3 to 0.8) than the previous reviews, organized based on the Ni content, as well as $LiNi_{1-x-y}Co_xAl_yO_2$ (0 < x, y < 1).

5.1 $LiNi_{1-x-y}TM_xTM'_yO_2$ (TM = Mn, TM' = Co)

Early compositional studies on systems with TM = Mn and TM' = Co were performed in the high Ni content region (1-x-y = 0.5 - 1). The partial substitution of Ni by both Mn and Co showed a positive effect on lithium stoichiometry (i.e., a reduction in defects involving Ni occupation of Li sites).[138, 139] For example, the transition metal content in the lithium layer fell from 7.2% to 2.4% when the Co content was increased from 0 to 0.3 in $LiCo_xMn_{0.2}Ni_{0.8-x}O_2$, even though the calcination was performed

in air rather than pure oxygen.[139] A Ni content between 0.7 and 0.75 was identified as the best in terms of capacity and cycle life, although initial capacities were only about 150 mAh/g using upper voltage cutoffs ranging from 4.2 to 4.3 V.[138, 139] In 2001, Ohzuku *et al.* reported the synthesis of $LiNi_{1/3}Mn_{1/3}Co_{1/3}O_2$ (NMC-333) by heating $LiOH \cdot H_2O$, $CoCO_3$, and a nickel manganese hydroxide at 1000 ^oC for 15h in air. This material delivered a discharge capacity of 150 mAh/g between 2.5 and 4.2 V and 200 mAh/g when the upper voltage limit was increased to 5 V in lithium half cells.[81] Later, a similar high rechargeable capacity was achieved upon cycling to 4.6 V by modifying the synthetic precursor to a triple hydroxide of Co, Ni, and Mn.[8] These exciting results prompted significant interest in optimizing the synthetic conditions, studying the physical properties, as well as establishing their relationships with electrochemical properties.

5.1.1 NMC-333

The early synthetic work on NMC-333 utilized solid-state reactions; e.g., high-temperature annealing of lithium salt and transition metal hydroxide and/or carbonate precursors; however, it was impossible to obtain a material free of a NiO impurity. Attempts to improve the phase-purity and uniformity of the cation distribution included various synthetic routes such as solid-state[81], sol-gel[9, 140], and modified co-precipitation of triple hydroxides[8, 138, 141]. Most NMC-333 samples that demonstrated good electrochemical performance were prepared around 900 ^oC, although the optimal temperature varied somewhat with the synthetic routes. After charging to 4.3V *vs.* Li^+/Li, a reversible capacity of 160 mAh/g is typically achieved, with capacities above 200 mAh/g obtained when a higher cutoff (≥ 4.6 V) is used, although this comes at the expense of capacity retention.[141-144]

The crystal and electronic structures of NMCs have been investigated by both first-principles calculations[145] and a suite of characterization techniques, i.e., high-resolution transmission electron microscopy (HRTEM),[146] neutron diffraction,[147] and nuclear magnetic resonance (NMR).[148] Although first principles calculations predicted that $LiNi_{1/3}Mn_{1/3}Co_{1/3}O_2$ should show transition metal ordering[10], only short-range ordering could be detected by the experimental methods. In NMC-333, Ni cations tend to be close to Mn cations in the first coordination shell, and Co cations are randomly distributed, according to neutron pair distribution function (PDF) analysis.[149] Due to size factors, anti-site mixing between Li and Co or Mn is less likely to occur than with Ni. The overall result is that NMC-333 has fewer of these defects than more Ni-rich compositions.[150] In addition, the valence states of transition metals in $LiNi_{1/3}Mn_{1/3}Co_{1/3}O_2$ differ from that of simple $LiMO_2$ (M = Ni, Mn, or Co) compositions, in which the oxidation states of the transition metals are 3+. Instead, the nominal oxidation states of Ni, Co, and Mn in pristine NMC-333 are 2+, 3+, and 4+, respectively.[9, 10, 149] Synchrotron x-ray absorption studies of the redox reaction mechanism during intercalation/deintercalation indicates that the main redox processes involve the Ni^{2+}/Ni^{4+} couple and that Mn^{4+} is electrochemically inactive.[9, 148, 151-154] The contribution of Co^{3+}/Co^{4+} redox processes is still a matter of debate; very little shift is observed in Co K-edges as a function of state-of-charge, instead, changes are observed in the O K-edge, suggesting that charge compensation occurs on O rather than Co. [9, 10, 145, 148] Chemical and structural
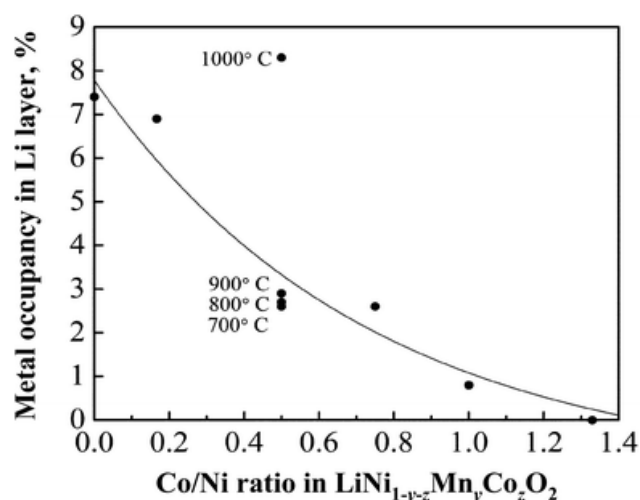
Figure 22 The occupancy of Ni in the Li layer as a function of Co/Ni ratio.[159] Used by with permission from reference 159.

stability studies performed on chemically delithiated NMC samples suggest that the initial $R\overline{3}m$ phase retains its original O3 stacking until about 0.7 Li per formula unit is de-intercalated. Extraction of more Li results in an irreversible change from O3 to O1 stacking (one layer of MO_2 sheets along c axis).[155-157] The overlap of oxygen 2p band and transition metal 3d bands means that, near the end of charge (4.5V vs. Li+/Li) oxygen can be oxidized, resulting in oxygen release.[13, 153] From these results, the optimum upper cutoff voltage for NMC was determined to be 4.3 - 4.4 V, falling within a range where non-aqueous electrolytes should be stable against oxidation by partially delithiated NMCs based on reactivity studies.[158]

5.1.2 $LiNi_xMn_yCo_zO_2$; $0.4 \leq x \leq 0.5$

In 2004, Whittingham's group investigated two series of compositions, $LiNi_{0.7-z}Mn_{0.3}Co_zO_2$ (z = 0.1, 0.3, 0.4) and $LiNi_{0.4}Mn_yCo_{0.6-y}$ (y = 0.2, 0.3, 0.4). Their study showed a positive effect of Co substitution on suppressing the migration of the transition metal into the Li site in the final products (**Figure 22**).[159] Of all the compounds studied, $LiNi_{0.4}Mn_{0.4}Co_{0.2}O_2$ showed the highest discharge capacity of about 180 mAh/g (2.5 - 4.3 V). Similar to NMC-333, the transition metals in $LiNi_{0.4}Mn_{0.4}Co_{0.2}O_2$ are present in the form of Ni^{2+}, Mn^{4+}, and Co^{3+}, and they are randomly distributed in the transition metal layers at room temperature.[160] Compositional studies within a narrower range ($0.33 \leq Ni = Mn \leq 0.5$, $0 \leq Co \leq 0.33$) confirmed that NMC-442 has the optimal transition metal content for superior electrochemical properties such as higher capacity, better thermal stability, and lower cost.[161, 162] Based on these results, cation substitution strategies have been employed to search for further improvements. A positive effect has been demonstrated by the partial substitution of Al and Ti for Co at low levels (≤ 0.05). Incorporation of electrochemically inactive Al decreases the discharge capacity, but improves the thermal and cycling stability.[163, 164] A beneficial structural effect of Al substitution is to limit the change in lattice parameters and local disordering during battery operation.[165, 166] Partial substitution of Ti for Co in both 333 and 442-type NMCs can delay the formation of surface rock-salt phase and improve the stability of NMC materials at a higher state-of-charge, resulting in an increased discharge capacity, lower first cycle inefficiency, and better cycling behavior to both 4.3 and 4.7 V vs. Li+/Li.[167-169]
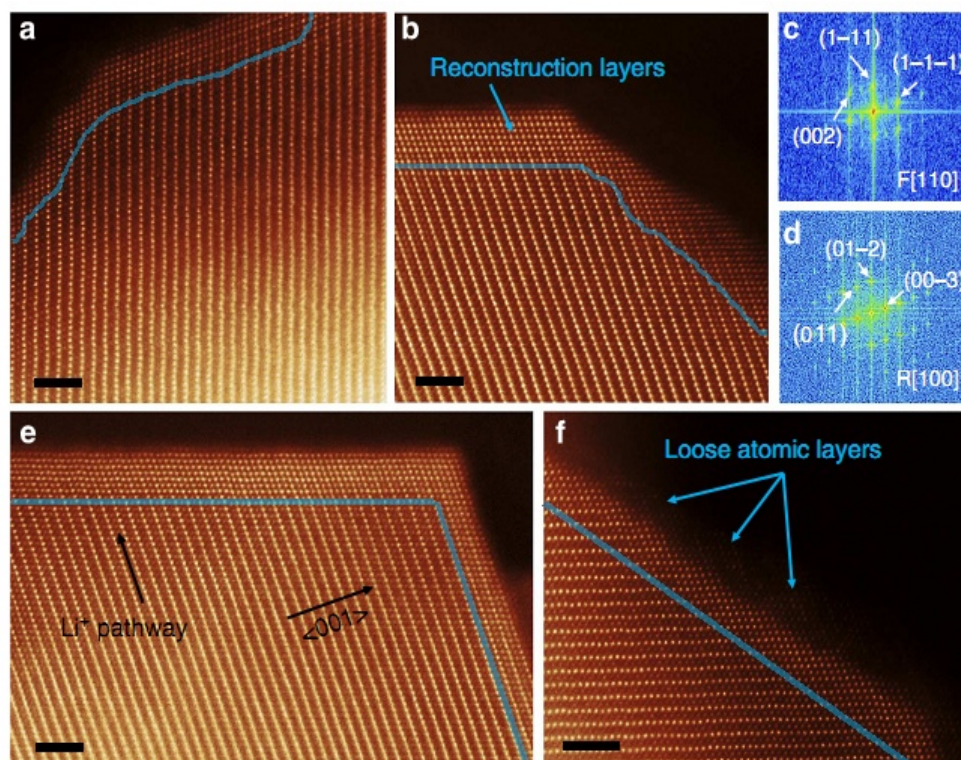
Figure 23 Atomic resolution annular dark-field (ADF) STEM images of $LiNi_{0.4}Mn_{0.4}Co_{0.2}O_2$ particles. (a) After electrolyte exposure for 30h (equivalent to the time for 1 cycle). (b) After 1 cycle (2.0 – 4.7 V). (c, d) FFT results showing the surface reconstruction layer ($Fm\overline{3}m$ [110] zone axis) shown in (b). (e) Surface reconstruction layer after 1 cycle (2.0 – 4.7 V). (f) Loose atomic layers on the surface after 1 cycle (2.0 – 4.7 V). The blue lines indicate the boundaries between the layered structure and surface reconstruction layer in all images. The scale bars are 2 nm in all images.[180] Used with permission from reference 180.

Compositions containing 50% Ni or more in the transition metal layer are commonly referred to as nickel-rich NMCs. The valence states of transition metals in the pristine oxides differ somewhat from those in NMC-333 and NMC-442. Because the Ni and Mn contents are not balanced in these compositions, charge neutrality is achieved by the partial oxidation of Ni^{2+} to Ni^{3+}.[170, 171] Studies on $LiCo_{0.5-y}Mn_{0.5-y}Ni_{2y}O_2$ ($0 \leq 2y \leq 1$) layered oxides show an increase in discharge capacity but more capacity fading as the Ni content is increased to 0.5 in cells operated up to 4.6 V.[172] Because of its high capacity, lower relative cost and good electrochemical performance, $LiNi_{0.5}Mn_{0.3}Co_{0.2}O_2$ is one of the most-studied compositions. It can deliver a high initial discharge capacity of 214 mAh/g (2.5 - 4.6 V vs. Li^+/Li) or 175 mAh/g (3 − 4.3 V vs. Li^+/Li) as well as good rate capability.[173] Recent electrochemical studies on $Li(Ni_{0.5}Mn_{0.3}Co_{0.2})O_2$ tend to emphasize higher upper voltage operation,[174-178] because of the possibility of achieving higher capacities and energy density. However, the capacity fading associated with high-voltage operation presents a significant challenge.

Advanced characterization techniques have been used to investigate the degradation mechanisms of NMCs cycled to high potentials. Surface reconstruction to disordered rock salt and/or spinel phases occurs in NMC-442 under a variety of conditions, including exposure to the electrolytic solution, but increases during cycling, especially to high potentials (**Figure 23**).[179, 180] Soft x-ray absorption spectroscopy experiments reveal that all three transition metals are more reduced than in the bulk in charged electrodes, implying that the disordered rock salt structure contains not only Ni, but Mn and Co as well. Such passivation layers that form on NMC compounds during high voltage cycling inhibit Li diffusion, the consequences of which are increased overall cell impedance and loss of practical capacity during cycling to high potentials. However, the lost capacity in NMC-442 cells can be nearly completely recovered during subsequent discharge at a low rate, indicating the significant effect of surface rather than bulk transformations on the electrochemical behavior.[180] The degree to which surface reconstruction and capacity fading occurs during high voltage cycling is a function not only of how the cycling is carried out (e.g., cyclic voltammetry vs. galvanostatic) but also of how the materials are synthesized, in particular, calcination time.[181] Other factors include the use of electrolyte additives, which affect both the cathode/electrolyte interface (CEI) and the passivation of the cathode surface. [178]

Similar to NMC-442, the irreversible surface phase transformation also occurs in NMC-532, the details of which depend on the cutoff voltage and is dominated by the transformation of the rhombohedral phase to spinel, with rock salt only observed during cycling to 4.8 V vs. Li^+/Li (**Figure 24**).[177] Furthermore, the disordered rock-salt surface phase observed by transmission electron microscopy/electron energy loss spectroscopy (TEM/EELS) on an NMC-532 after long-term cycling vs. $Li_4Ti_5O_{12}$ (> 4000 cycles) appeared to involve primarily reduction of Mn^{4+} to Mn^{2+}.[174] In contrast to NMC-333, which undergoes a phase transformation from O3 to O1 at high-states of charge (Section 4.1.1), the O1 phase was not detected during delithiation of NMC-532, probably because there is less sliding of the slabs due to the higher degree of Li-Ni exchange.[177]

5.1.3 $LiNi_xMn_yCo_zO_2$; $0.6 \leq x \leq 0.8$

While greater capacities can be obtained by cycling cells containing NMCs to higher potentials, side reactions with electrolytic solutions and effects of surface reconstruction result in suboptimal cycling behavior. Increasing the nickel content to values as high as x = 0.6 - 0.8 can lead to higher practical capacities at moderate operating potentials but it is not clear if this comes at the expense of thermal stability at high states-of-charge.[182-186] The increased Ni content also presents challenges for synthesis, because of the high Ni^{3+} content.

For compositions with x = 0.6, a number of synthetic methods including combustion, co-precipitation, spray pyrolysis, and solid-state reactions have been attempted. At an optimal synthesis condition (800 - 900 °C in O_2), the best samples can deliver an initial capacity of about 170 mAh/g when charged to 4.3 V vs. Li^+/Li.[187-192] For $LiNi_{0.6}Co_{0.4-x}Mn_xO_2$, Mn and Co content influence both physical and electrochemical properties. For example, the primary particle size of final products increases as the Co content rises (Co = 0.05 - 0.2), suggesting accelerated grain growth.[189, 191] For compositions

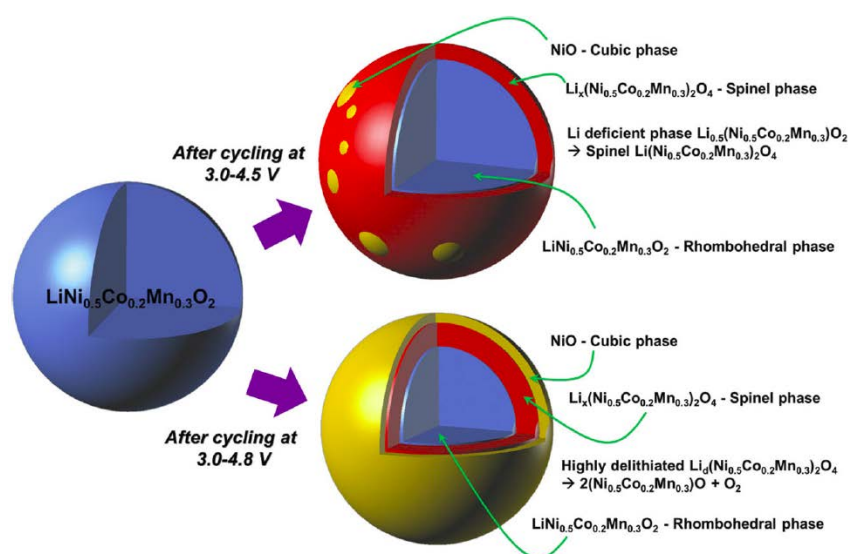**Figure 24** Degradation mechanism of $LiNi_{0.5}Mn_{0.3}Co_{0.2}O_2$ showing the phase transformation after cycling tests under high-voltage operations.[177] Used with permission from reference 177.
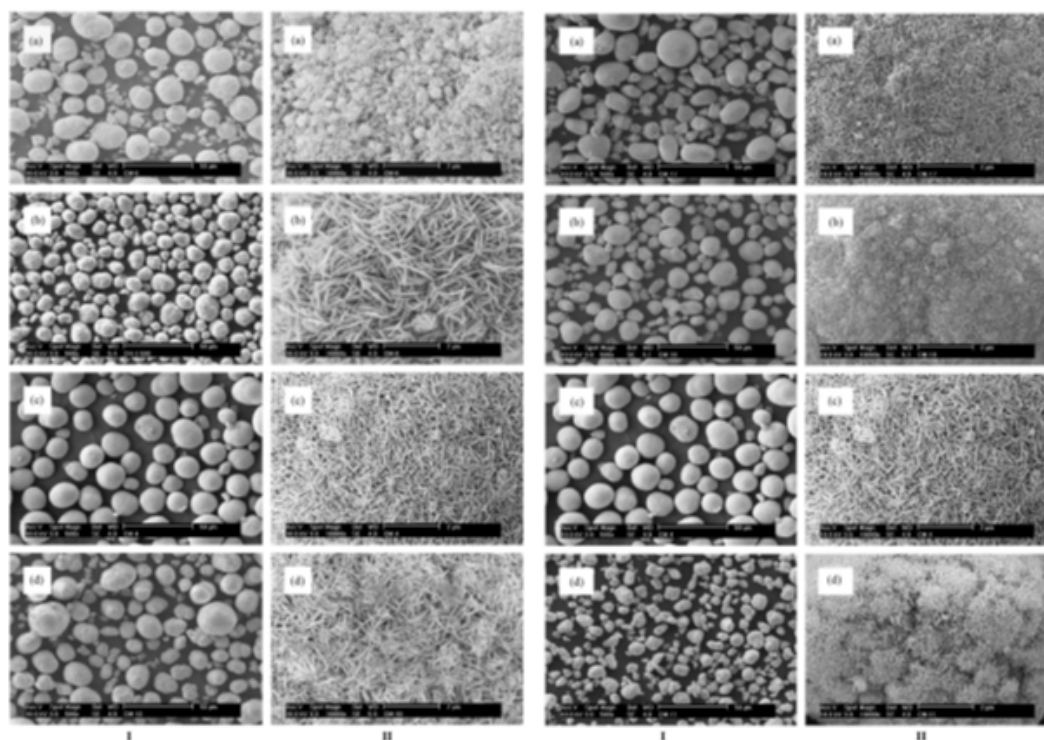
Figure 25 SEM images of $Ni_{0.8}Co_{0.15}Mn_{0.05}(OH)_2$ powders demonstrating pH effect (left panel): (a) 9.5 - 10, (b) 11.2 - 11.3, (c) 11.5 - 11.6, (d) 11.9 - 12.0; and NH_3: metal molar ratio effect (right panel): (a) 0.6, (b) 0.8, (c) 1.0, (d) 1.2. (Magnification: I 500 X, II 10,000X).[200] Used with permission from reference 200.

over a wider and finer range (Co = 0.05 - 0.3, step size = 0.05), $LiNi_{0.6}Co_{0.2}Mn_{0.2}O_2$ containing identical Co and Mn content had the highest tap density (2.32 g/cc for $LiNi_{0.6}Co_{0.2}Mn_{0.2}O_2$).[190] Increasing the Co content leads to higher capacities but the cycling performance deteriorates. $LiNi_{0.6}Mn_{0.2}Co_{0.2}O_2$ exhibits the best balance between reversible capacity and capacity retention as well as the smallest polarization. In the dq/dV plots of $LiNi_{0.6}Mn_{1-x}Co_xO_2$ (x = 0.05 – 0.3, 2.8 – 4.5 V vs. Li^+/Li), only one pair of redox peaks appeared in the potential range of 3.7 – 4.1 V.[190] In-situ XRD studies on $Li_{1-x}Ni_{0.6}Mn_{0.15}Co_{0.25}O_2$ electrodes (3 – 4.5 V vs. Li^+/Li) showed no new H2 phase formation upon Li deintercalation, instead, only a solid-solution reaction with a small lattice volume change (4%) prevailed during the charge-discharge processes.[193]

Samples with Ni contents of x= 0.7 [194-196] and x= 0.8 [186, 197-206] that are prepared under optimal synthesis conditions can deliver high initial discharge capacities of about 180, and 190 mAh/g using an upper voltage cutoff of 4.3 V cutoff in lithium half cells, respectively. This capacity can be further increased to > 200 mAh/g after charging to 4.5 V for both x = 0.7, and 0.8 compositions.[207, 208] The synthesis of Ni-rich NMCs is complex and requires optimization of several parameters to produce materials with good performance. Synthetic variables under study ranged from details of the precursor preparation such as the amount of lithium excess to the best annealing temperature, duration, and atmosphere. For example, $LiNi_{0.7}Mn_{0.15}Co_{0.15}O_2$ compounds using 5 mol% Li excess exhibited the highest capacity and best cycling performance among materials prepared by a solvothermal method. This sample had the lowest amount of Ni^{2+}/Li^+ mixing (4.6% Ni^{2+} in Li layer and 1.7% Li^+ in TM layer) and the largest inter slab space, which accounted for its good performance.[195] For materials made by co-precipitation, the conditions strongly influenced

the particle morphology and tap density, because of differences in the reaction rate (**Figure 25**). Smooth and spherical particles with the highest tap density (2.72 g/cc) were produced when the optimal conditions of NH_3: metal molar ratio of 1.0 and a pH range of 11.5 - 11.6 were used. [200] Spray pyrolysis using citric acid (CA) and ethylene glycol (EG) complexing agents has also been employed to prepare $LiNi_{0.8}Co_{0.15}Mn_{0.05}O_2$. Additives, amount of lithium excess, and annealing conditions were varied, all of which demonstrated significant effects on the electrochemical performance (**Figure 26**). The best sample, which demonstrated a high initial discharge capacity (218 mAh/g) and an excellent cycling performance (98% capacity retention @ cycle 50) in lithium half cells (2.8 – 4.5 V) was synthesized with 6 mol% Li excess and 0.3 M each CA and EG, and annealed at 800 °C in O_2 for 3h. The complexing agents ensured homogeneity of the transition metals and enabled the complete decomposition of reactants inside the reactor. The use of excess Li compensated for Li loss during preparation and heat treatment processes.[207] These examples show how critical details of the synthesis are for preparation of high-performance Ni-rich layered oxides; minor adjustments of the parameters strongly influence morphology, stoichiometry and defect structure.[197, 209]

A composition study within a very narrow range revealed that the cycling stability of $LiNi_{0.8-x}Co_{0.1}Mn_{0.1+x}O_2$ (0 ≤ x ≤ 0.08) was significantly improved when Mn content was increased; 85.7% for $LiNi_{0.72}Co_{0.1}Mn_{0.18}O_2$ vs. 64% for $LiNi_{0.8}Co_{0.1}Mn_{0.1}O_2$ @ cycle 100 (2.7– 4.5 V vs. Li^+/Li). This improvement was ascribed to the stabilization of the electrode/electrolyte interfaces as evidenced by the lower charge-transfer resistance in the electrochemical impedance spectra of $Li_{0.72}Co_{0.1}Mn_{0.18}O_2$ electrode, implying less surface film formation.[208] Although
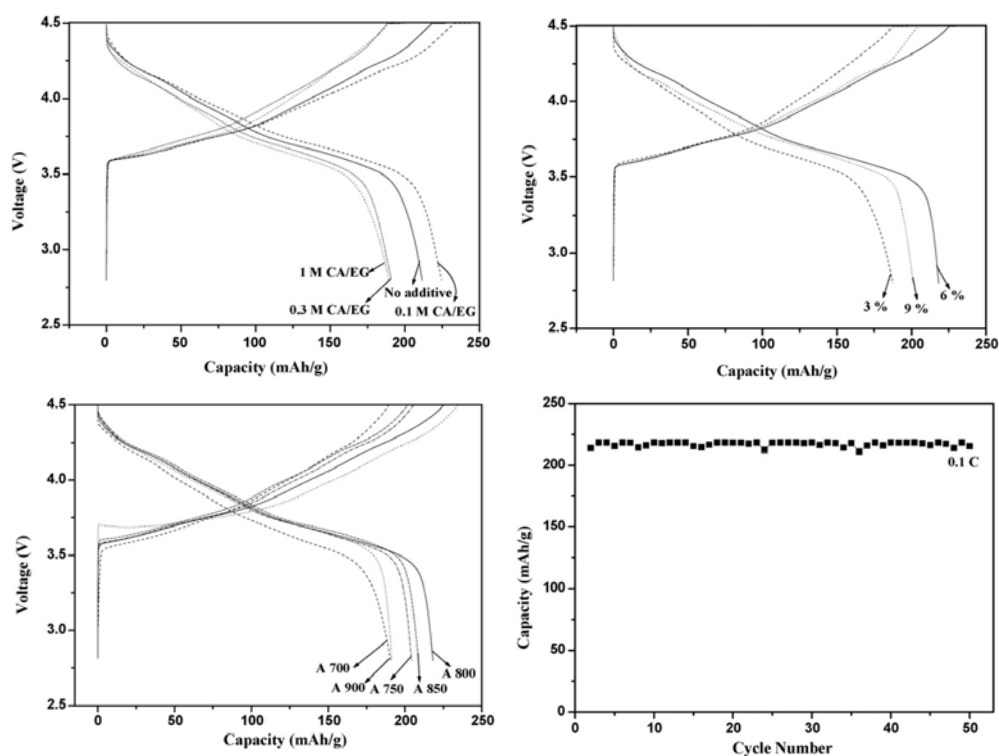
Figure 26 Initial voltage profiles of $LiNi_{0.8}Co_{0.15}Mn_{0.05}O_2$ cathodes synthesized by spray pyrolysis in lithium half-cells (4.5 – 2.8 V, 0.1C), indicating the effects of (a) polymeric precursor, (b) Li excess, (c) annealing temperature, and (d) cycling performance of the material annealed at 800 °C.[207] Used with permission from reference 207.

these Ni-rich layered oxides can deliver a high initial capacity and good cycle life when modified to contain more Mn, they still suffer from long-term cycling and thermal instabilities and are sensitive to moisture. An exothermic reaction occurs around 220 °C for $LiNi_{0.8}Co_{0.1}Mn_{0.1}O_2$ charged to 4.3 V.[210] A phase transformation appears to occur from layered $R\overline{3}m$ to spinel $Fd\overline{3}m$ at 200 °C, and to $Fm\overline{3}m$ rock salt at 250 °C when heating charged $Li_{0.2}Ni_{0.8}Mn_{0.1}Co_{0.1}O_2$ electrodes.[186] Similar phenomena in the phase transformation of Ni-rich layered cathodes was also observed during storage at 90 °C after charge of the $LiNi_{0.8}Co_{0.1+x}Mn_{0.1-x}O_2$ electrode to 4.3 V vs. Li⁺/Li. These conditions led to the reduction of Ni^{4+} to Ni^{3+} although the Mn oxidation state remained at +4. Additionally, charged cathodes stored at 90 °C for 7 days transformed into a spinel phase ($Fd\overline{3}m$).[202, 206] Parasitic reactions between the highly reactive charged electrode surface and electrolytic solutions were

proposed to be the main reason for the failure of $Li_{0.8}Co_{0.1}Mn_{0.1}O_2$ electrode cycled at a voltage > 4.2 V.[211]

5.1.4 New Material Design Concepts for NMCs

In order to counteract the high capacity and poor structural stability of high Ni content NMCs, a new material design concept based on a core-shell structure has recently been demonstrated. A concentration-gradient layered oxide consisting of a high-energy Ni-rich layered oxide (Ni: Mn: Co = 0.8: 0.1: 0.1) in the bulk surrounded by a less reactive Ni-poor outer layer (Ni: Mn: Co = 0.08: 0.46: 0.46), was prepared by a two-step co-precipitation method, with the goal of providing robust surface protection when in contact with electrolyte (**Figure 27**).[210, 212, 213] An as-prepared concentration-gradient layered oxide with a nominal global composition of $LiNi_{0.64}Mn_{0.18}Co_{0.18}O_2$ demonstrated a high initial capacity of 209 mAh/g with about 200 mAh/g retained after 500 cycles at 55 °C between 3 and 4.4 V vs. Li⁺/Li. This material had improved safety
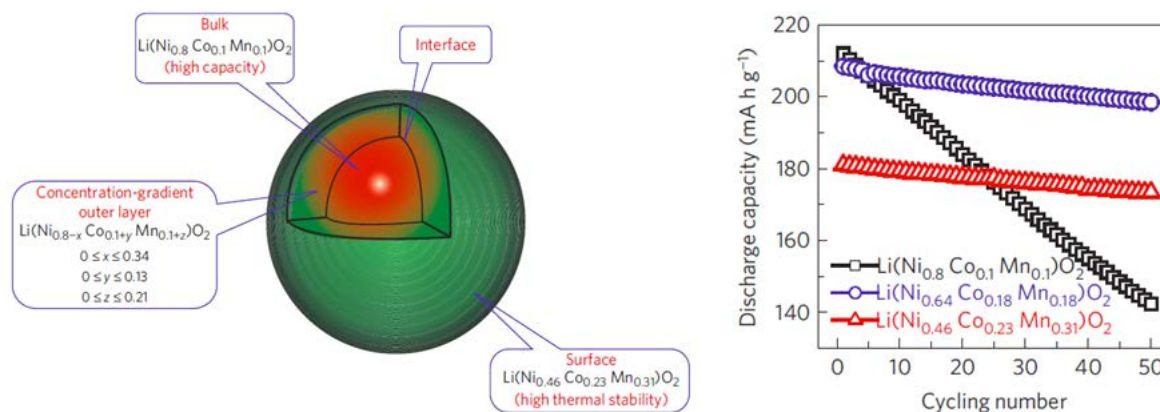

Figure 27 (a) Schematic diagram of electrode with Ni-rich core surrounded by concentration-gradient outer layer. (b) Cycling performance of $Li[Ni_{0.8}Co_{0.1}Mn_{0.1}]O_2$, $Li[Ni_{0.46}Co_{0.23}Mn_{0.31}]O_2$ and concentration-gradient material (4.4 – 3.0 V, 0.5C, 55 °C).[210] Used with permission from reference 210.
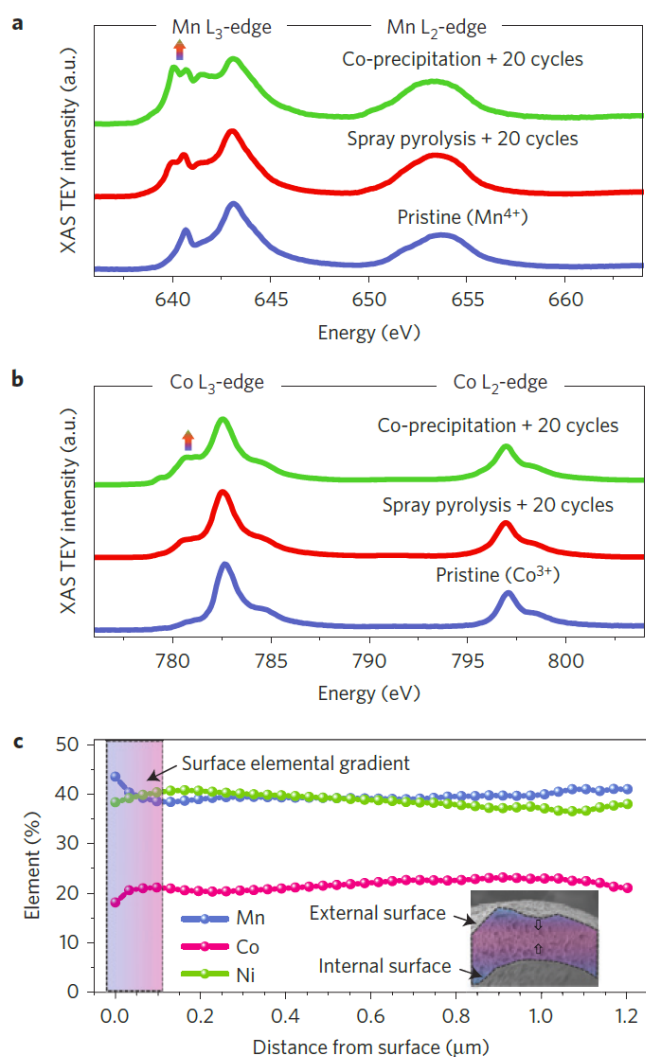
Figure 28 Soft XAS spectra of Mn L-edge (a) and Co L-edge (b) of NMC-442 prepared conventionally and by spray pyrolysis after 20 cycles in lithium half cells to 4.7 V. Results indicate less reduced transition metal on the surfaces of the electrode made by spray pyrolysis than on the one made conventionally after cycling, implying less surface reconstruction. (c) Elemental distribution as a function of the distance from the particle surface calculated using TXM data.[211] Used with permission from reference 211.

characteristics evidenced by an onset reaction temperature ~ 90 °C higher, with 31% less heat generated, than a homogeneous $LiNi_{0.8}Mn_{0.1}Co_{0.1}O_2$ electrode. Recently, a hierarchically structured NMC-442 cathode with a graded composition on both the primary and secondary particle levels was prepared by spray pyrolysis. The local elemental segregation, which resulted in Ni-poor surfaces resulted in superior resistance to surface reconstruction compared to conventionally prepared materials with homogeneous distributions of transition metals (**Figure 28**).[211] These examples suggest it is possible to improve the performance of Ni-rich NMCs by engineering particle surfaces to reduce reactivity.

5.2 $LiNi_{1-x-y}TM_xTM'_yO_2$ (Tm = Co, Tm' = Al, 1-x-y = 0.8)

Layered lithium transition metal oxides containing a combination of Ni, Co, and Al are already used in commercial Li-ion batteries and can be considered quite mature in their development. Recent rapid advancement and development of new characterization techniques have lent new insights into the functioning of these materials, such as the fading mechanism. The advantages of the $LiNi_{1-x}Co_xO_2$ (0 ≤ x ≤1) system over $LiNiO_2$ and $LiCoO_2$ have been previously discussed in

the section on layered oxides containing two transition metals; these can be summarized as reduction of defects leading to improved performance over $LiNiO_2$, as well as lower cost than $LiCoO_2$. The impetus for partial Al substitution came from the need to improve the thermal stability of the Ni and Co containing oxides, and was based on observations made on layered Ni oxides partially substituted with Al (*vide infra*). The thermal stabilization by partial Al substitution is ascribed to the stability of Al^{3+} in tetrahedral sites, which disrupts the cation migration necessary for the phase transformations that occur at elevated temperatures.[41, 101, 214]

Substitution of electrochemically inactive Al for electroactive Ni cations intrinsically limits the maximal amount of Li that can be extracted from the structure, potentially preventing overcharge. If the substitution is too great, there is a substantial decrease in reversible capacity, and impurities are formed. The solid solution limit appears to be 0 ≤ y ≤ 0.1. For this reason, studies on the $LiNi_{1-x-y}Co_xAl_yO_2$ (0 ≤x, y ≤1) system have mainly focused on compositions with low Al contents (5 - 10 %).[215-217] In 2002, SAFT reported a significant improvement in both electrochemical performance and safety characteristics in large Li-ion batteries using $LiNi_{0.8}Co_{0.15}Al_{0.05}O_2$ cathodes over those containing $LiNiO_2$. This composition is considered to be optimal and is commonly designated NCA.[6, 215, 218-220]

Synchrotron *in-situ* XRD studies revealed that NCA cathodes undergo similar phase transformations as $LiNiO_2$ during the 1st charge, including H1 to H2 hexagonal phase transformations early in the charge process, and H3 phase formation at the end of charge. However, the H3 phase formation was significantly suppressed compared to $LiNiO_2$, leading to superior thermal stability in the overcharged state.[221] Due to these favorable characteristics, NCA cathodes have been successfully utilized in batteries for electric vehicles made by Tesla Motors, which uses ~7000 of Panasonic's cylindrical 18650 cells in the battery pack.[222-224] Despite its commercial success, battery cells using NCA cathode still suffer from capacity fade and impedance rise after long-term cycling, particularly at high temperatures, and there are still some safety concerns.

Studies directed towards understanding the origins of capacity fading and impedance rise in cells with NCA cathodes indicate that, in some scenarios, the capacity and power fade of a battery is mainly due to the degradation of the NCA cathode rather than the graphite anode (3.0 - 4.1 V, 80 °C, 2C).[225] The degradation includes structural and chemical changes of the cathode, electrolyte decomposition, formation of passivating surface layers, loss of electronic contact, and gas evolution. Raman and atomic force microscopy (AFM) studies revealed inconsistencies in the kinetic behavior of individual NCA particles (rate of charge/discharge varying with time and location) and an increase in the surface composition ratio of NCA to carbon in the composite electrodes upon cell aging and cycling. Such carbon retreat or rearrangement may result in the loss of contact of active materials with the carbon matrix, therefore, contributing to cathode interfacial charge-transfer impedance, power and capacity loss.[226-228]

Structural and chemical change studies on $LiNi_{0.8}Co_{0.2}O_2$ cathodes cycled in a full cell using a suite of TEM, EELS, and XAS techniques showed evidence for a < 5 nm NiO-type surface layer after the formation cycle, the growth of which may be responsible
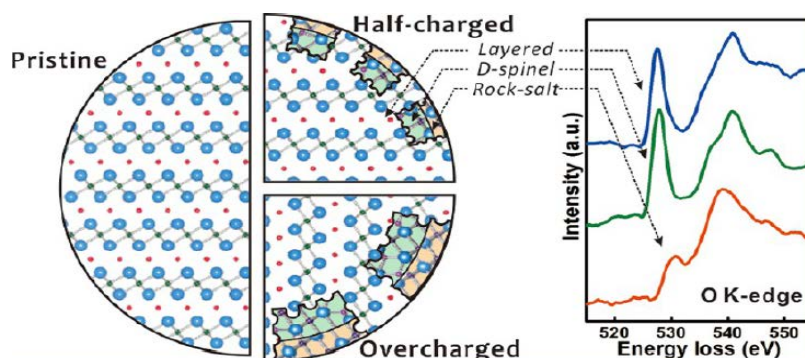
Figure 29 Schematic summarizing the crystallographic and electronic structure changes (O K-edge EELS) that occurs in NCA cathode upon charge.[235] Used with permission from reference 235.

for the impedance rise observed during the accelerated cycling test (holding cells at temperatures ranging from 40 to 70 °C).[229] Similar impedance rises were also observed on aged NCA cathodes under typical HEV conditions (5C rate, 40 °C) after 5250 deep cycles.[224] The Ni L-edge and O K-edge XAS studies on cycled NCA electrodes in the discharged state (1000 cycles, 60 °C) suggested that there was a substantial amount of Ni^{2+} on the NCA surface in contrast to the Ni^{3+} observed in the bulk.[225] Combined with TEM- EELS imaging, this was evidence for a NiO-like rock salt phase on the surface. In addition, formation of Li- and O-deficient areas was observed in the cycled samples, which could be due to Li substitution on Ni sites in the NiO-like degraded phase and oxygen loss during cycling.[230-232] When NCA cathodes were cycled at elevated temperature (80 °C), quantitative analysis on the energy shift of Ni K-edge XANES spectra showed a strong positive correlation between the capacity fade and the valence state of the Ni ion.[225] This phase evolution from a layered structure in the bulk to a NiO-like phase on the surface was also observed in cathodes from a commercial 18650-type Li-ion battery.

A number of experiments on the phase transformation and gas evolution have been performed to understand the safety characteristics of NCA cathodes. Release of oxygen can initiate thermal runaway at a fairly low temperature because of the presence of flammable components in the electrolytic solution. Most studies focused on the evolution of the average crystallographic structure of the NCA cathode as a function of temperature and state-of-charge,

which significantly affects the thermal stability of the charged NCA cathode. It was first shown by detailed TEM analysis that the overcharged $Li_xNi_{0.8}Co_{0.15}Al_{0.05}O_2$ (x < 0.15) cathode contains a complex core-shell-surface structure consisting of a layered $R\bar{3}m$ core, a spinel shell, and a rock-salt structure at the surface.[183] Moreover, this phase transition occurs at a low temperature for electrodes in the charged state. The development of the disordered spinel structure ($Fd\bar{3}m$) in some particles occurs at temperatures below 100 °C and the disordered rock-salt structure ($Fm\bar{3}m$) was observed at a temperature above 200 °C.[233, 234] A combination of TEM, selected area electron diffraction (SAED) and EELS techniques provides additional insights (**Figure 29**). The crystal structure changes from layered $R\bar{3}m$ to spinel $Fd\bar{3}m$ to rock-salt $Fm\bar{3}m$ occurs due to movement of ions that result in the modification of the nearby coordination and bonding with oxygen, and correlates with significant changes in electronic structure of oxygen. During deintercalation, reduction of Ni and an increase in the effective electron density of oxygen cause a charge imbalance, leading to the formation of oxygen vacancies and the development of surface porosity.[233, 235, 236] Direct evidence of concomitant phase transformation and gas evolution (O_2, CO_2) was detected using *in situ* time-resolved XRD (TR-XRD) coupled with mass spectroscopy (MS) (**Figure 30**).[236] Because of the direct relationship between the degree of Li extraction, the initiation of phase transitions, and the highly deleterious loss of oxygen from the structure, it is clear that

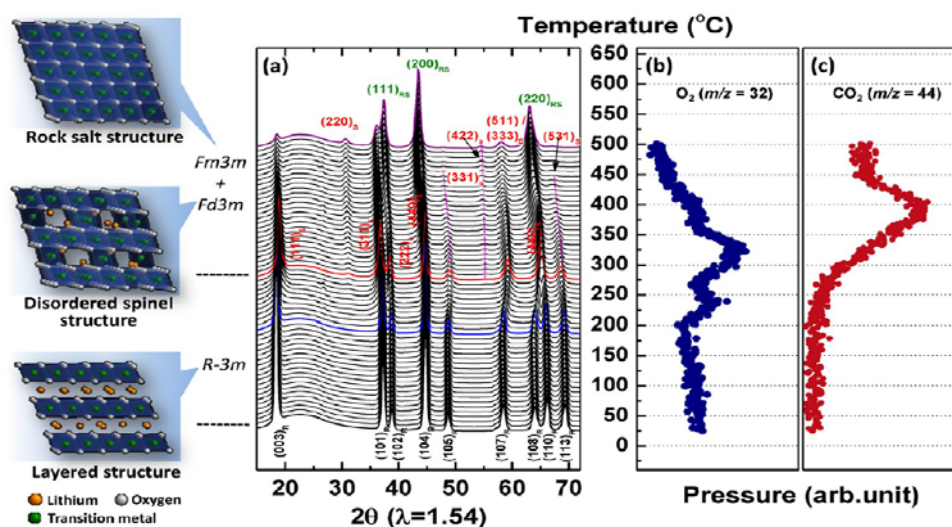**Figure 30** (a) TR-XRD patterns and in-situ mass spectra for (b) O_2 and (c) CO_2 when heating $Li_{0.5}Ni_{0.8}Co_{0.15}Al_{0.05}O_2$ up to 500 °C. The left panels show the crystal structure of rhombohedral, spinel, and rock salt.[236] Used with permission from reference 236.

improvements to the overall performance of these materials must occur through improvements in surface engineering as well as enhanced control over the kinetics of lithium intercalation and deintercalation.[235, 237-240]

6. Future Directions

High-performance NCA and NMC cathodes have evolved from many thousands of hours of research over the last two decades, devoted to understanding complex relationships among compositions, structures, physical, and electrochemical properties. The approach has largely been empirical, although understanding has grown with time and improvements in synthesis and characterization techniques. A reasonable question to ask is whether this process can be hastened in order to identify new better-performing materials for next-generation batteries, especially given the high potential growth of the electric vehicle and grid storage markets and their associated technical demands. In particular, there is a great need for new technologies that allow quicker design of new materials and performance optimization. Traditional approaches for battery material development rely heavily on trial-and-error. In contrast, a combinatorial materials approach could offer faster and more efficient methods of identifying promising advanced materials, which are likely to be more complex than their predecessors (e.g., containing multiple substituents, phase mixtures, gradient compositions, etc.). Depending on the synthetic method integrated into the combinatorial approach, the typical library outputs are thin films made by deposition techniques, and powders based on solution-based reactions such as co-precipitation. The as-produced thin films are thin enough that the electrochemical properties can be directly obtained in binder and carbon additive-free configurations to obtain a first approximation of electrochemical behavior. To date, thin film based combinatorial methods have mostly been employed to screen compositions in various ternary metal/metal oxide libraries for the development of Li-ion anodes[241, 242] and solid electrolytes.[243]. However, Dahn's group recently adopted a solution-based combinatorial approach to map out the entire composition ranges within the Li-Mn-Ni-O, Li-Mn-Co-O, and Li-Mn-Al-O chemical spaces using high-throughput XRD for phase identification.[244-247] Many types of structures (rock salt, spinel, and layered compounds, etc.), as well as phase mixtures, occur in these quaternary systems. This rapid screening technique allowed construction of a detailed phase diagram so that researchers can concentrate on compositions most likely to result in a high degree of electroactivity. Combinatorial studies on the electrochemistry of as-produced powder samples would be ideal and enable a better understanding of composition-structure-property relationships, as such results may be more relevant to bulk material properties compared to thin films. This requires further development of a reliable and cost-effective process that simulates standard electrode formulations and can bind the powders to current collectors.

Combinatorial approaches may be particularly helpful in identifying useful Li-excess materials, which recent first principal calculations have identified as potential high capacity, high performance cathodes. For example, Lee *et al.* reported a new layered oxide, $Li_{1.211}Mo_{0.467}Cr_{0.3}O_2$, which delivered a high reversible capacity (> 250 mAh/g, 4.3 – 1.5 V vs. Li+/Li, C/20) even after it

transformed to a disordered rock salt after a few cycles.[248] Since then, several new cathode materials with disordered rock-salt structures (Li_2VO_2F[249], Li_3NbO_4-based systems[250, 251], $Li_{1.2}Ni_{0.333}Ti_{0.333}Mo_{0.1333}O_2$[252], and $Li_{1.333}Ni_{0.333}Mo_{0.333}O_2$[253]) have been reported to have high electrochemical activity. These disordered rock salts possess the same atomic arrangements as well-ordered layered lithium metal oxide cathodes (e.g., $LiCoO_2$) but lithium and transition metals are randomly distributed in the sublattices. Until recently, materials like this have been overlooked as potential Li-ion cathode candidates because of this feature. The *ab initio* computational results show that the key to designing good disordered materials is having a large enough Li-excess to ensure a percolating network of diffusional channels *via* octahedron - tetrahedron - octahedron Li hopping.[248] This percolation theory opens up a vast compositional space of disordered lithium metal oxides. Using a combinatorial approach will allow for composition screenings of large libraries to rapidly identify the most promising disordered rocksalt-type lithium metal oxides.

7. Summary and Remarks

Ni-containing layered oxides are technologically important cathode materials for Li-ion batteries. Early work focused on $LiNiO_2$ because of the structural similarity to $LiCoO_2$, the first successful oxide cathode. Synthesis of high-performance $LiNiO_2$ proved difficult due to the tendency to form lithium-deficient defective structures ($Li_{1-x}Ni_{1+x}O_2$) with Ni^{2+} ions in the van der Waals gaps. In addition, structural and thermal instability at high states-of-charge led to safety concerns and prompted researchers to investigate strategies to solve these problems. Intensive investigation of the effects of partial substitution of one or more elements led to the development of two important classes of Ni-containing layered oxides, NMCs and NCA, which are in use today. Partial substitution of Co for Ni in NCA reduced the number of defects and the addition of Al improved the thermal stability. NCA is now the cathode of choice in batteries for electric vehicles (Tesla) although safety concerns have not been entirely alleviated. NMC cathodes have also been intensively scrutinized, with the battery community gradually adopting compositions with high Ni content such as NMC-532, NMC-622, or NMC-811, because these materials deliver large practical capacities at moderate potentials. Reactivity of the high Ni-content electrodes with electrolytic solutions and the thermal behavior at high states-of-charge, which lead to capacity fading and safety issues, are still a concern. However, ingenious methods to allay the effects of surface reactivity, such as sophisticated synthesis methods that reduce the amount of Ni on particle surfaces have now been demonstrated. This, in combination with other approaches such as electrolyte additives and robust coatings to ameliorate the ill effects of reactivity, should allow adoption of high-capacity electrodes in Li-ion batteries for many applications, in particular, cost-sensitive electric vehicles.

We have witnessed the progression of layered lithium metal oxide cathodes from the simpler single transition metal layered oxides such as $LiNiO_2$ to variants substituted with one, two, or more elements. This process ultimately resulted in the advanced NCA and NMC cathodes used today, and allowed composition-structure-performance relationships to be

developed. The advent of new material design principles now offer a new category of disordered rocksalt-type lithium metal oxides, with potentially very high capacities, to explore. The compositional space of interest is potentially very large, which ordinarily would require large investments of time and work using conventional methods to identify the most promising candidates. In contrast, combinatorial approaches, which allow for rapid screening of large libraries of compositions within a given system, should allow rapid identification of materials of interest.

Acknowledgements

References

1. M. S. Whittingham, *Chemical Reviews*, 2004, **104**, 4271-4301.
2. W. Liu, P. Oh, X. Liu, M.-J. Lee, W. Cho, S. Chae, Y. Kim and J. Cho, *Angewandte Chemie International Edition*, 2015, **54**, 4440-4457.
3. A. Manthiram, A. Vadivel Murugan, A. Sarkar and T. Muraliganth, *Energy & Environmental Science*, 2008, **1**, 621-638.
4. A. Kraytsberg and Y. Ein-Eli, *Advanced Energy Materials*, 2012, **2**, 922-939.
5. P. Kalyani and N. Kalaiselvi, *Science and Technology of Advanced Materials*, 2005, **6**, 689-703.
6. C. H. Chen, J. Liu, M. E. Stoll, G. Henriksen, D. R. Vissers and K. Amine, *Journal of Power Sources*, 2004, **128**, 278-285.
7. K. S. Kang, Y. S. Meng, J. Breger, C. P. Grey and G. Ceder, *Science*, 2006, **311**, 977-980.
8. N. Yabuuchi and T. Ohzuku, *Journal of Power Sources*, 2003, **119–121**, 171-174.
9. B. J. Hwang, Y. W. Tsai, D. Carlier and G. Ceder, *Chemistry of Materials*, 2003, **15**, 3676-3682.
10. Y. Koyama, I. Tanaka, H. Adachi, Y. Makimura and T. Ohzuku, *Journal of Power Sources*, 2003, **119–121**, 644-648.
11. J. R. Dahn, U. Vonsacken and C. A. Michal, *Solid State Ionics*, 1990, **44**, 87-97.
12. K. Kang, C. H. Chen, B. J. Hwang and G. Ceder, *Chemistry of Materials*, 2004, **16**, 2685-2690.
13. Y. S. Meng and M. Elena Arroyo-de Dompablo, *Energy & Environmental Science*, 2009, **2**, 589-609.
14. B. L. Ellis, K. T. Lee and L. F. Nazar, *Chemistry of Materials*, 2010, **22**, 691-714.
15. M. S. Whittingham, *Chemical Reviews*, 2014, **114**, 11414-11443.
16. C. Li, H. P. Zhang, L. J. Fu, H. Liu, Y. P. Wu, E. Ram, R. Holze and H. Q. Wu, *Electrochimica Acta*, 2006, **51**, 3872-3883.
17. W. Li, J. N. Reimers and J. R. Dahn, *Solid State Ionics*, 1993, **67**, 123-130.
18. W. Li, J. N. Reimers and J. R. Dahn, *Physical Review B*, 1992, **46**, 3236-3246.
19. T. Ohzuku and Y. Makimura, *Research on Chemical Intermediates*, 2006, **32**, 507-521.
20. C. Pouillerie, E. Suard and C. Delmas, *Journal of Solid State Chemistry*, 2001, **158**, 187-197.
21. A. N. Mansour, X. Q. Yang, X. Sun, J. McBreen, L. Croguennec and C. Delmas, *Journal of the Electrochemical Society*, 2000, **147**, 2104-2109.
22. C. Delmas, J. P. Peres, A. Rougier, A. Demourgues, F. Weill, A. Chadwick, M. Broussely, F. Perton, P. Biensan and P. Willmann, *Journal of Power Sources*, 1997, **68**, 120-125.
23. A. Rougier, P. Gravereau and C. Delmas, *Journal of the Electrochemical Society*, 1996, **143**, 1168-1175.
24. W. Ebner, D. Fouchard and L. Xie, *Solid State Ionics*, 1994, **69**, 238-256.
25. Z. H. Lu, X. J. Huang, H. Huang, L. Q. Chen and J. Schoonman, *Solid State Ionics*, 1999, **120**, 103-107.
26. C. H. Lu and L. Wei-Cheng, *Journal of Materials Chemistry*, 2000, **10**, 1403-1407.
27. T. Ohzuku, A. Ueda, M. Nagayama, Y. Iwakoshi and H. Komori, *Electrochimica Acta*, 1993, **38**, 1159-1167.
28. I. Davidson, J. E. Greedan, U. von Sacken, C. A. Michal and J. R. Dahn, *Solid State Ionics*, 1991, **46**, 243-247.
29. S. N. Kwon, J. H. Song and D. R. Mumm, *Ceramics International*, 2011, **37**, 1543-1548.
30. M. Song, I. Kwon, H. Kim, S. Shim and D. R. Mumm, *Journal of Applied Electrochemistry*, 2006, **36**, 801-805.
31. M. M. Rao, C. Liebenow, M. Jayalakshmi, H. Wulff, U. Guth and F. Scholz, *Journal of Solid State Electrochemistry*, 2001, **5**, 348-354.
32. N. Kalaiselvi, A. V. Raajaraajan, B. Sivagaminathan, N. G. Renganathan, N. Muniyandi and M. Ragavan, *Ionics*, 2003, **9**, 382-387.
33. T. Ohzuku, A. Ueda and M. Nagayama, *Journal of The Electrochemical Society*, 1993, **140**, 1862-1870.
34. R. Kanno, H. Kubo, Y. Kawamoto, T. Kamiyama, F. Izumi, Y. Takeda and M. Takano, *Journal of Solid State Chemistry*, 1994, **110**, 216-225.
35. C. Delmas and L. Croguennec, *Mrs Bulletin*, 2002, **27**, 608-612.
36. H. Arai, S. Okada, H. Ohtsuka, M. Ichimura and J. Yamaki, *Solid State Ionics*, 1995, **80**, 261-269.
37. J. Xu, F. Lin, D. Nordlund, E. J. Crumlin, F. Wang, J. Bai, M. M. Doeff and W. Tong, *Chemical Communications*, 2016, **52**, 4239-4242.
38. J. N. Reimers, W. Li and J. R. Dahn, *Physical Review B*, 1993, **47**, 8486-8493.
39. K. S. Park, S. H. Park, Y. K. Sun, K. S. Nahm, Y. S. Lee and M. Yoshio, *Journal of Applied Electrochemistry*, 2002, **32**, 1229-1233.
40. X. Q. Yang, X. Sun and J. McBreen, *Electrochemistry Communications*, 1999, **1**, 227-232.
41. M. Guilmard, L. Croguennec, D. Denux and C. Delmas, *Chemistry of Materials*, 2003, **15**, 4476-4483.
42. C. Delmas, M. Ménétrier, L. Croguennec, S. Levasseur, J. P. Pérès, C. Pouillerie, G. Prado, L. Fournès and F. Weill, *International Journal of Inorganic Materials*, 1999, **1**, 11-19.
43. K. Chang, B. Hallstedt and D. Music, *Calphad*, 2012, **37**, 100-107.
44. K. Dokko, M. Nishizawa, S. Horikoshi, T. Itoh, M. Mohamedi and I. Uchida, *Electrochemical and Solid State Letters*, 2000, **3**, 125-127.
45. W. Li, J. N. Reimers and J. R. Dahn, *Solid State Ionics*, 1993, **67**, 123-130.
46. I. Nakai, K. Takahashi, Y. Shiraishi, T. Nakagome, F. Izumi, Y. Ishii, F. Nishikawa and T. Konishi, *Journal of Power Sources*, 1997, **68**, 536-539.
47. I. Nakai, K. Takahashi, Y. Shiraishi, T. Nakagome and F. Nishikawa, *Journal of Solid State Chemistry*, 1998, **140**, 145-148.
48. A. N. Mansour, J. McBreen and C. A. Melendres, *Journal of the Electrochemical Society*, 1999, **146**, 2799-2809.
49. H. S. Liu, Z. R. Zhang, Z. L. Gong and Y. Yang, *Electrochemical and Solid State Letters*, 2004, **7**, A190-A193.
50. S. H. Kang and M. M. Thackeray, *Electrochemistry Communications*, 2009, **11**, 748-751.
51. M. G. Kim and J. Cho, *Journal of Materials Chemistry*, 2008, **18**, 5880-5887.
52. N. Imanishi, K. Shizuka, T. Ikenishi, T. Matsumura, A. Hirano and Y. Takeda, *Solid State Ionics*, 2006, **177**, 1341-1346.
53. R. E. Ruther, H. Zhou, C. Dhital, K. Saravanan, A. K. Kercher, G. Y. Chen, A. Huq, F. M. Delnick and J. Nanda, *Chemistry of Materials*, 2015, **27**, 6746-6754.

54. H. Park, T. Yoon, Y.-U. Kim, J. H. Ryu and S. M. Oh, *Electrochimica Acta*, 2013, **108**, 591-595.

55. H. Lee, S.-K. Chang, E.-Y. Goh, J.-Y. Jeong, J. H. Lee, H.-J. Kim, J.-J. Cho and S.-T. Hong, *Chemistry of Materials*, 2008, **20**, 5-7.

56. R. Kanno, T. Shirane, Y. Inaba and Y. Kawamoto, *Journal of Power Sources*, 1997, **68**, 145-152.

57. C. Delmas and I. Saadoune, *Solid State Ionics*, 1992, **53**, 370-375.

58. M. Balasubramanian, X. Sun, X. Q. Yang and J. McBreen, *Journal of Power Sources*, 2001, **92**, 1-8.

59. K. Mukai, J. Sugiyama, Y. Ikedo, J. H. Brewer, E. J. Ansaldo, G. D. Morris, K. Ariyoshi and T. Ohzuku, *Journal of Power Sources*, 2007, **174**, 843-846.

60. B. Banov, J. Bourilkov and M. Mladenov, *Journal of Power Sources*, 1995, **54**, 268-270.

61. E. Zhecheva and R. Stoyanova, *Solid State Ionics*, 1993, **66**, 143-149.

62. H. Arai, S. Okada, Y. Sakurai and J. Yamaki, *Solid State Ionics*, 1998, **109**, 295-302.

63. A. Rougier, I. Saadoune, P. Gravereau, P. Willmann and C. Delmas, *Solid State Ionics*, 1996, **90**, 83-90.

64. T. Ohzuku and R. J. Brodd, *Journal of Power Sources*, 2007, **174**, 449-456.

65. M. Balasubramanian, X. Sun, X. Q. Yang and J. McBreen, *Journal of the Electrochemical Society*, 2000, **147**, 2903-2909.

66. A. Kinoshita, K. Yanagida, A. Yanai, Y. Kida, A. Funahashi, T. Nohma and I. Yonezu, *Journal of Power Sources*, 2001, **102**, 283-287.

67. W. Li and C. Currie, *Journal of the Electrochemical Society*, 1997, **144**, 2773-2779.

68. D. Caurant, N. Baffier, B. Garcia and J. P. PereiraRamos, *Solid State Ionics*, 1996, **91**, 45-54.

69. C. Jaephil, J. HyunSook, P. YoungChul, GeunBae and L. Hong Sup, *Journal of the Electrochemical Society*, 2000, **147**, 15-20.

70. B. V. R. Chowdari, G. V. S. Rao and S. Y. Chow, *Solid State Ionics*, 2001, **140**, 55-62.

71. G. T. K. Fey, R. F. Shiu, V. Subramanian, J. G. Chen and C. L. Chen, *Journal of Power Sources*, 2002, **103**, 265-272.

72. Z. X. Yang, B. Wang, W. S. Yang and X. Wei, *Electrochimica Acta*, 2007, **52**, 8069-8074.

73. I. Saadoune and C. Delmas, *Journal of Solid State Chemistry*, 1998, **136**, 8-15.

74. I. Saadoune, M. Menetrier and C. Delmas, *Journal of Materials Chemistry*, 1997, **7**, 2505-2511.

75. P. Wilk, J. Marzec and J. Molenda, *Solid State Ionics*, 2003, **157**, 109-114.

76. R. V. Chebiam, F. Prado and A. Manthiram, *Journal of Solid State Chemistry*, 2002, **163**, 5-9.

77. B. J. Hwang, R. Santhanam and C. H. Chen, *Journal of Power Sources*, 2003, **114**, 244-252.

78. J. Cho and B. Park, *Journal of Power Sources*, 2001, **92**, 35-39.

79. I. Saadoune and C. Delmas, *Journal of Materials Chemistry*, 1996, **6**, 193-199.

80. E. Rossen, C. D. W. Jones and J. R. Dahn, *Solid State Ionics*, 1992, **57**, 311-318.

81. T. Ohzuku and Y. Makimura, *Chemistry Letters*, 2001, **30**, 642-643.

82. Y. Makimura and T. Ohzuku, *Journal of Power Sources*, 2003, **119–121**, 156-160.

83. T. Ohzuku and Y. Makimura, *Chemistry Letters*, 2001, 744-745.

84. Z. H. Lu, D. D. MacNeil and J. R. Dahn, *Electrochemical and Solid State Letters*, 2001, **4**, A200-A203.

85. S. Jouanneau, D. D. MacNeil, Z. Lu, S. D. Beattie, G. Murphy and J. R. Dahn, *Journal of the Electrochemical Society*, 2003, **150**, A1299-A1304.

86. W.-S. Yoon, Y. Paik, X.-Q. Yang, M. Balasubramanian, J. McBreen and C. P. Grey, *Electrochemical and Solid-State Letters*, 2002, **5**, A263-A266.

87. S. Venkatraman and A. Manthiram, *Chemistry of Materials*, 2003, **15**, 5003-5009.

88. Y. Arachi, H. Kobayashi, S. Emura, Y. Nakata, M. Tanaka and T. Asai, *Chemistry Letters*, 2003, **32**, 60-61.

89. S. Venkatraman, J. Choi and A. Manthiram, *Electrochemistry Communications*, 2004, **6**, 832-837.

90. K. Kang and G. Ceder, *Physical Review B*, 2006, **74**, 7.

91. Y. Hinuma, Y. S. Meng, K. Kang and G. Ceder, *Chemistry of Materials*, 2007, **19**, 1790-1800.

92. H. Kobayashi, H. Sakaebe, H. Kageyama, K. Tatsumi, Y. Arachi and T. Kamiyama, *Journal of Materials Chemistry*, 2003, **13**, 590-595.

93. Y. K. Sun, D. J. Lee, Y. J. Lee, Z. H. Chen and S. T. Myung, *Acs Applied Materials & Interfaces*, 2013, **5**, 11434-11440.

94. Z. H. Lu and J. R. Dahn, *Journal of the Electrochemical Society*, 2001, **148**, A710-A715.

95. J. M. Paulsen, C. L. Thomas and J. R. Dahn, *Journal of the Electrochemical Society*, 2000, **147**, 861-868.

96. J. M. Paulsen, D. Larcher and J. R. Dahn, *Journal of the Electrochemical Society*, 2000, **147**, 2862-2867.

97. J. M. Paulsen and J. R. Dahn, *Journal of The Electrochemical Society*, 2000, **147**, 2478-2485.

98. G. Ceder, Y. M. Chiang, D. R. Sadoway, M. K. Aydinol, Y. I. Jang and B. Huang, *Nature*, 1998, **392**, 694-696.

99. M. K. Aydinol, A. F. Kohan, G. Ceder, K. Cho and J. Joannopoulos, *Physical Review B*, 1997, **56**, 1354-1365.

100. Y. I. Jang, B. Huang, Y. M. Chiang and D. R. Sadoway, *Electrochemical and Solid-State Letters*, 1998, **1**, 13-16.

101. Y.-I. Jang, B. Huang, H. Wang, G. R. Maskaly, G. Ceder, D. R. Sadoway, Y.-M. Chiang, H. Liu and H. Tamura, *Journal of Power Sources*, 1999, **81–82**, 589-593.

102. S. Buta, D. Morgan, A. Van der Ven, M. K. Aydinol and G. Ceder, *Journal of the Electrochemical Society*, 1999, **146**, 4335-4338.

103. M. Guilmard, A. Rougier, A. Grune, L. Croguennec and C. Delmas, *Journal of Power Sources*, 2003, **115**, 305-314.

104. E. Shinova, E. Zhecheva and R. Stoyanova, *Journal of Solid State Chemistry*, 2006, **179**, 3151-3158.

105. R. Stoyanova, E. Zhecheva, E. Kuzmanova, R. Alcantara, P. Lavela and J. L. Tirado, *Solid State Ionics*, 2000, **128**, 1-10.

106. L. Cai, Z. Liu, K. An and C. Liang, *Journal of the Electrochemical Society*, 2012, **159**, A924-A928.

107. L. Croguennec, Y. Shao-Horn, A. Gloter, C. Colliex, M. Guilmard, F. Fauth and C. Delmas, *Chemistry of Materials*, 2009, **21**, 1051-1059.

108. Q. M. Zhong and U. Vonsacken, *Journal of Power Sources*, 1995, **54**, 221-223.

109. S. H. Park, K. S. Park, Y. K. Sun, K. S. Nahm, Y. S. Lee and M. Yoshio, *Electrochimica Acta*, 2001, **46**, 1215-1222.

110. T. Ohzuku, T. Yanagawa, M. Kouguchi and A. Ueda, *Journal of Power Sources*, 1997, **68**, 131-134.

111. T. Ohzuku, A. Ueda and M. Kouguchi, *Journal of the Electrochemical Society*, 1995, **142**, 4033-4039.

112. A. Urban, J. Lee and G. Ceder, *Advanced Energy Materials*, 2014, **4**, n/a-n/a.

113. G. Prado, L. Fournes and C. Delmas, *Solid State Ionics*, 2000, **138**, 19-30.

114. C. Delmas, G. Prado, A. Rougier, E. Suard and L. Fournès, *Solid State Ionics*, 2000, **135**, 71-79.

115. E. Chappel, G. Chouteau, G. Prado and C. Delmas, *Solid State Ionics*, 2003, **159**, 273-278.

116. G. Prado, E. Suard, L. Fournes and C. Delmas, *Journal of Materials Chemistry*, 2000, **10**, 2553-2560.

117. G. Prado, A. Rougier, L. Fournes and C. Delmas, *Journal of the Electrochemical Society*, 2000, **147**, 2880-2887.

118. P. Mohan and G. P. Kalaignan, *Journal of Electroceramics*, 2013, **31**, 210-217.

119. S. Ho Chang, S.-G. Kang, S.-W. Song, J.-B. Yoon and J.-H. Choy, *Solid State Ionics*, 1996, **86–88, Part 1**, 171-175.

120. J. W. Joeng and S.-G. Kang, *Journal of Power Sources*, 2003, **123**, 75-78.

121. L. Croguennec, E. Suard, P. Willmann and C. Delmas, *Chemistry of Materials*, 2002, **14**, 2149-2157.

122. K. Kang, D. Carlier, J. Reed, E. M. Arroyo, G. Ceder, L. Croguennec and C. Delmas, *Chemistry of Materials*, 2003, **15**, 4503-4507.

123. S. Ho Chang, S.-G. Kang, S.-W. Song, J.-B. Yoon and J.-H. Choy, *Solid State Ionics*, 1996, **86–88, Part 1**, 171-175.

124. H. Arai, S. Okada, Y. Sakurai and J. Yamaki, *Journal of the Electrochemical Society*, 1997, **144**, 3117-3125.

125. J. Kim and K. Amine, *Electrochemistry Communications*, 2001, **3**, 52-55.

126. J. Kim and K. Amine, *Journal of Power Sources*, 2002, **104**, 33-39.

127. J. Kim, J. Liu, C. Chen and K. Amine, *Journal of the Electrochemical Society*, 2003, **150**, A1491-A1497.

128. H.-W. Ha, K. H. Jeong and K. Kim, *Journal of Power Sources*, 2006, **161**, 606-611.

129. S. N. Kwon, H. R. Park and M. Y. Song, *Ceramics International*, 2014, **40**, 11131-11137.

130. Y. Nishida, Y. Nakane and T. Satoh, *Journal of Power Sources*, 1997, **68**, 561-564.

131. X. Ma, K. Kang, G. Ceder and Y. S. Meng, *Journal of Power Sources*, 2007, **173**.

132. C. Julien, G. A. Nazri and A. Rougier, *Solid State Ionics*, 2000, **135**, 121-130.

133. C. Pouillerie, L. Croguennec, P. Biensan, P. Willmann and C. Delmas, *Journal of The Electrochemical Society*, 2000, **147**, 2061-2069.

134. A. R. Naghash and J. Y. Lee, *Electrochimica Acta*, 2001, **46**, 2293-2304.

135. A. R. Naghash and J. Y. Lee, *Electrochimica Acta*, 2001, **46**, 941-951.

136. P. He, H. Yu, D. Li and H. Zhou, *Journal of Materials Chemistry*, 2012, **22**, 3680-3695.

137. R. Robert, C. Villevieille and P. Novak, *Journal of Materials Chemistry A*, 2014, **2**, 8589-8598.

138. Z. L. Liu, A. S. Yu and J. Y. Lee, *Journal of Power Sources*, 1999, **81**, 416-419.

139. M. Yoshio, H. Noguchi, J. Itoh, M. Okada and T. Mouri, *Journal of Power Sources*, 2000, **90**, 176-181.

140. C.-H. Chen, C.-J. Wang and B.-J. Hwang, *Journal of Power Sources*, 2005, **146**, 626-629.

141. K. M. Shaju, G. V. Subba Rao and B. V. R. Chowdari, *Electrochimica Acta*, 2002, **48**, 145-151.

142. I. Belharouak, Y. K. Sun, J. Liu and K. Amine, *Journal of Power Sources*, 2003, **123**, 247-252.

143. N. Yabuuchi, Y. Makimura and T. Ohzuku, *Journal of The Electrochemical Society*, 2007, **154**, A314-A321.

144. S. L. Wu, W. Zhang, X. Song, A. K. Shukla, G. Liu, V. Battaglia and V. Srinivasan, *Journal of the Electrochemical Society*, 2012, **159**, A438-A444.

145. Y. Koyama, N. Yabuuchi, I. Tanaka, H. Adachi and T. Ohzuku, *Journal of The Electrochemical Society*, 2004, **151**, A1545-A1551.

146. N. Yabuuchi, Y. Koyama, N. Nakayama and T. Ohzuku, *Journal of The Electrochemical Society*, 2005, **152**, A1434-A1440.

147. P. S. Whitfield, I. J. Davidson, L. M. D. Cranswick, I. P. Swainson and P. W. Stephens, *Solid State Ionics*, 2005, **176**, 463-471.

148. Y. Won-Sub, C. P. Grey, M. Balasubramanian, Y. Xiao-Qing, D. A. Fischer and J. McBreen, *Electrochemical and Solid-State Letters*, 2004, **7**, A53-A55.

149. D. Zeng, J. Cabana, J. Bréger, W. S. Yoon and C. P. Grey, *Chemistry of Materials*, 2007, **19**, 6277-6289.

150. S. Lee and S. S. Park, *Journal of Physical Chemistry C*, 2012, **116**, 6484-6489.

151. J.-M. Kim and H.-T. Chung, *Electrochimica Acta*, 2004, **49**, 937-944.

152. H. Kobayashi, Y. Arachi, S. Emura, H. Kageyama, K. Tatsumi and T. Kamiyama, *Journal of Power Sources*, 2005, **146**, 640-644.

153. Y. W. Tsai, B. J. Hwang, G. Ceder, H. S. Sheu, D. G. Liu and J. F. Lee, *Chemistry of Materials*, 2005, **17**, 3191-3199.

154. M. Labrini, I. Saadoune, F. Scheiba, A. Almaggoussi, J. Elhaskouri, P. Amoros, H. Ehrenberg and J. Brötz, *Electrochimica Acta*, 2013, **111**, 567-574.

155. A. Manthiram and J. Choi, *Journal of Power Sources*, 2006, **159**, 249-253.

156. J. Choi and A. Manthiram, *Journal of the Electrochemical Society*, 2005, **152**, A1714-A1718.

157. S. C. Yin, Y. H. Rho, I. Swainson and L. F. Nazar, *Chemistry of Materials*, 2006, **18**, 1901-1910.

158. Y. Wang, J. Jiang and J. R. Dahn, *Electrochemistry Communications*, 2007, **9**, 2534-2540.

159. J. K. Ngala, N. A. Chernova, M. M. Ma, M. Mamak, P. Y. Zavalij and M. S. Whittingham, *Journal of Materials Chemistry*, 2004, **14**, 214-220.

160. M. Ma, N. A. Chernova, B. H. Toby, P. Y. Zavalij and M. S. Whittingham, *Journal of Power Sources*, 2007, **165**, 517-534.

161. Z. Li, N. A. Chernova, M. Roppolo, S. Upreti, C. Petersburg, F. M. Alamgir and M. S. Whittingham, *Journal of The Electrochemical Society*, 2011, **158**, A516-A522.

162. S. W. Oh, S. H. Park, C. W. Park and Y. K. Sun, *Solid State Ionics*, 2004, **171**, 167-172.

163. L. Croguennec, J. Bains, J. Breger, C. Tessier, P. Biensan, S. Levasseur and C. Delmas, *Journal of the Electrochemical Society*, 2011, **158**, A664-A670.

164. J. Bains, L. Croguennec, J. Breger, F. Castaing, S. Levasseur, C. Delmas and P. Biensan, *Journal of Power Sources*, 2011, **196**, 8625-8631.

165. T. E. Conry, A. Mehta, J. Cabana and M. M. Doeff, *Chemistry of Materials*, 2012, **24**, 3307-3317.

166. T. E. Conry, A. Mehta, J. Cabana and M. M. Doeff, *Journal of The Electrochemical Society*, 2012, **159**, A1562-A1571.

167. K. C. Kam, A. Mehta, J. T. Heron and M. M. Doeff, *Journal of The Electrochemical Society*, 2012, **159**, A1383-A1392.

168. I. M. Markus, F. Lin, K. C. Kam, M. Asta and M. M. Doeff, *The Journal of Physical Chemistry Letters*, 2014, **5**, 3649-3655.

169. S. Wolff-Goodrich, F. Lin, I. M. Markus, D. Nordlund, H. L. Xin, M. Asta and M. M. Doeff, *Physical Chemistry Chemical Physics*, 2015, **17**, 21778-21781.

170. D. Li, Y. Sasaki, K. Kobayakawa and Y. Sato, *Electrochimica Acta*, 2006, **51**, 3809-3813.

171. D. C. Li, Y. Sasaki, M. Kageyama, K. Kobayakawa and Y. Sato, *Journal of Power Sources*, 2005, **148**, 85-89.

172. J. Choi and A. Manthiram, *Journal of Power Sources*, 2006, **162**, 667-672.

173. S. Yang, X. Wang, X. Yang, Y. Bai, Z. Liu, H. Shu and Q. Wei, *Electrochimica Acta*, 2012, **66**, 88-93.

174. H. Kuriyama, H. Saruwatari, H. Satake, A. Shima, F. Uesugi, H. Tanaka and T. Ushirogouchi, *Journal of Power Sources*, 2015, **275**, 99-105.

175. K. Liu, G. L. Yang, Y. Dong, T. Shi and L. Chen, *Journal of Power Sources*, 2015, **281**, 370-377.

176. W. B. Hua, J. B. Zhang, Z. Zheng, W. Y. Liu, X. H. Peng, X. D. Guo, B. H. Zhong, Y. J. Wang and X. L. Wang, *Dalton Transactions*, 2014, **43**, 14824-14832.

177. S.-K. Jung, H. Gwon, J. Hong, K.-Y. Park, D.-H. Seo, H. Kim, J. Hyun, W. Yang and K. Kang, *Advanced Energy Materials*, 2014, **4**.

178. Y.-M. Lee, K.-M. Nam, E.-H. Hwang, Y.-G. Kwon, D.-H. Kang, S.-S. Kim and S.-W. Song, *The Journal of Physical Chemistry C*, 2014, **118**, 10631-10639.

179. F. Lin, D. Nordlund, I. M. Markus, T.-C. Weng, H. L. Xin and M. M. Doeff, *Energy & Environmental Science*, 2014, **7**, 3077-3085.

180. F. Lin, I. M. Markus, D. Nordlund, T.-C. Weng, M. D. Asta, H. L. Xin and M. M. Doeff, *Nature Communications*, 2014, **5**.

181. F. Lin, D. Nordlund, T. Pan, I. M. Markus, T.-C. Weng, H. L. Xin and M. M. Doeff, *Journal of Materials Chemistry A*, 2014, **2**, 19833-19840.

182. S. M. Bak, E. Y. Hu, Y. N. Zhou, X. Q. Yu, S. D. Senanayake, S. J. Cho, K. B. Kim, K. Y. Chung, X. Q. Yang and K. W. Nam, *Acs Applied*

Materials & Interfaces, 2014, **6**, 22594-22601.

183.   L. Wu, N. Kyung-Wan, X. Wang, Y. Zhou, J.-C. Zheng, X.-Q. Yang and Y. Zhu, *Chemistry of Materials*, 2011, **23**, 3953-3960.

184.   Y. Kim, *ACS Applied Materials & Interfaces*, 2012, **4**, 2329-2333.

185.   H. Konishi, T. Yuasa and M. Yoshikawa, *Journal of Power Sources*, 2011, **196**, 6884-6888.

186.   H. Konishi, M. Yoshikawa and T. Hirano, *Journal of Power Sources*, 2013, **244**, 23-28.

187.   L. Liang, K. Du, Z. Peng, Y. Cao, J. Duan, J. Jiang and G. Hu, *Electrochimica Acta*, 2014, **130**, 82-89.

188.   P. Yue, Z. Wang, H. Guo, F. Wu, Z. He and X. Li, *Journal of Solid State Electrochemistry*, 2012, **16**, 3849-3854.

189.   P. Y. Liao, J. G. Duh and S. R. Sheen, *Journal of Power Sources*, 2005, **143**, 212-218.

190.   L. W. Liang, K. Du, W. Lu, Z. D. Peng, Y. B. Cao and G. R. Hu, *Electrochimica Acta*, 2014, **146**, 207-217.

191.   J. Li, L. Wang, Q. Zhang and X. He, *Journal of Power Sources*, 2009, **189**, 28-33.

192.   W. Ahn, S. N. Lim, K. N. Jung, S. H. Yeon, K. B. Kim, H. S. Song and K. H. Shin, *Journal of Alloys and Compounds*, 2014, **609**, 143-149.

193.   P. Y. Liao, J. G. Duh and H. S. Sheu, *Electrochemical and Solid-State Letters*, 2007, **10**, A88-A92.

194.   L. Liang, G. Hu, Y. Cao, K. Du and Z. Peng, *Journal of Alloys and Compounds*, 2015, **635**, 92-100.

195.   C. C. Fu, G. S. Li, D. Luo, Q. Li, J. M. Fan and L. P. Li, *Acs Applied Materials & Interfaces*, 2014, **6**, 15822-15831.

196.   Y. K. Sun, D. H. Kim, H. G. Jung, S. T. Myung and K. Amine, *Electrochimica Acta*, 2010, **55**, 8621-8627.

197.   J. H. Shim, C. Y. Kim, S. W. Cho, A. Missiul, J. K. Kim, Y. J. Ahn and S. Lee, *Electrochimica Acta*, 2014, **138**, 15-21.

198.   S. W. Woo, S. T. Myung, H. Bang, D. W. Kim and Y. K. Sun, *Electrochimica Acta*, 2009, **54**, 3851-3856.

199.   S. S. Jan, S. Nurgul, X. Q. Shi, H. Xia and H. Pang, *Electrochimica Acta*, 2014, **149**, 86-93.

200.   K. K. Cheralathan, N. Y. Kang, H. S. Park, Y. J. Lee, W. C. Choi, Y. S. Ko and Y. K. Park, *Journal of Power Sources*, 2010, **195**, 1486-1494.

201.   S. U. Woo, C. S. Yoon, K. Amine, I. Belharouak and Y. K. Sun, *Journal of the Electrochemical Society*, 2007, **154**, A1005-A1009.

202.   J. Eom, M. G. Kim and J. Cho, *Journal of the Electrochemical Society*, 2008, **155**, A239-A245.

203.   C. Hua, K. Du, C. Tan, Z. Peng, Y. Cao and G. Hu, *Journal of Alloys and Compounds*, 2014, **614**, 264-270.

204.   S. G. Woo, J. H. Han, K. J. Kim, J. H. Kim, J. S. Yu and Y. J. Kim, *Electrochimica Acta*, 2015, **153**, 115-121.

205.   M. H. Kim, H. S. Shin, D. Shin and Y. K. Sun, *Journal of Power Sources*, 2006, **159**, 1328-1333.

206.   X. H. Xiong, Z. X. Wang, P. Yue, H. J. Guo, F. X. Wu, J. X. Wang and X. H. Li, *Journal of Power Sources*, 2013, **222**, 318-325.

207.   S. H. Ju and Y. C. Kang, *Ceramics International*, 2009, **35**, 1633-1639.

208.   J. M. Zheng, W. H. Kan and A. Manthiram, *Acs Applied Materials & Interfaces*, 2015, **7**, 6926-6934.

209.   M. S. Idris and A. R. West, *Journal of the Electrochemical Society*, 2012, **159**, A396-A401.

210.   Y. K. Sun, S. T. Myung, B. C. Park, J. Prakash, I. Belharouak and K. Amine, *Nature Materials*, 2009, **8**, 320-324.

211.   F. Lin, D. Nordlund, Y. Li, M. K. Quan, L. Cheng, T.-C. Weng, Y. Liu, H. L. Xin and M. M. Doeff, *Nature Energy*, 2016, **1**, 15004.

212.   Y.-K. Sun, S.-T. Myung, M.-H. Kim, J. Prakash and K. Amine, *Journal of the American Chemical Society*, 2005, **127**, 13411-13418.

213.   Y.-K. Sun, S.-T. Myung, H.-S. Shin, Y. C. Bae and C. S. Yoon, *The Journal of Physical Chemistry B*, 2006, **110**, 6810-6815.

214.   M. Guilmard, L. Croguennec and C. Delmas, *Chemistry of Materials*, 2003, **15**, 4484-4493.

215.   M. Guilmard, C. Pouillerie, L. Croguennec and C. Delmas, *Solid State Ionics*, 2003, **160**, 39-50.

216.   S. Madhavi, G. V. Subba Rao, B. V. R. Chowdari and S. F. Y. Li, *Journal of Power Sources*, 2001, **93**, 156-162.

217.   M. Jo, M. Noh, P. Oh, Y. Kim and J. Cho, *Advanced Energy Materials*, 2014, **4**, 8.

218.   P. Kalyani, N. Kalaiselvi, N. G. Renganathan and M. Raghavan, *Materials Research Bulletin*, 2004, **39**, 41-54.

219.   S. B. Majumder, S. Nieto and R. S. Katiyar, *Journal of Power Sources*, 2006, **154**, 262-267.

220.   S. H. Ju, H. C. Jang and Y. C. Kang, *Electrochimica Acta*, 2007, **52**, 7286-7292.

221.   W.-S. Yoon, K. Y. Chung, J. McBreen and X.-Q. Yang, *Electrochemistry Communications*, 2006, **8**, 1257-1262.

222.   C. Martin, *Nature Nanotechnology*, 2014, **9**, 327-328.

223.   A. Trippe, T. Massier and T. Hamacher, *2013 IEEE Energytech*, 2013, DOI: 10.1109/EnergyTech.2013.6645338, 6 pp.-6 pp.

224.   Y. Zhang and C.-Y. Wang, *Journal of the Electrochemical Society*, 2009, **156**, A527-A535.

225.   T. Sasaki, T. Nonaka, H. Oka, C. Okuda, Y. Itou, Y. Kondo, Y. Takeuchi, Y. Ukyo, K. Tatsumi and S. Muto, *Journal of The Electrochemical Society*, 2009, **156**, A289-A293.

226.   J. Lei, F. McLarnon and R. Kostecki, *The Journal of Physical Chemistry B*, 2005, **109**, 952-957.

227.   R. Kostecki, J. Lei, F. McLarnon, J. Shim and K. Striebel, *Journal of The Electrochemical Society*, 2006, **153**, A669-A672.

228.   R. Kostecki and F. McLarnon, *Electrochemical and Solid-State Letters*, 2004, **7**, A380-A383.

229.   D. P. Abraham, R. D. Twesten, M. Balasubramanian, J. Kropf, D. Fischer, J. McBreen, I. Petrov and K. Amine, *Journal of the Electrochemical Society*, 2003, **150**, A1450-A1456.

230.   S. Muto, Y. Sasano, K. Tatsumi, T. Sasaki, K. Horibuchi, Y. Takeuchi and Y. Ukyo, *Journal of The Electrochemical Society*, 2009, **156**, A371-A377.

231.   Y. Kojima, S. Muto, K. Tatsumi, H. Kondo, H. Oka, K. Horibuchi and Y. Ukyo, *Journal of Power Sources*, 2011, **196**, 7721-7727.

232.   S. Muto, K. Tatsumi, T. Sasaki, H. Kondo, T. Ohsuna, K. Horibuchi and Y. Takeuchi, *Electrochemical and Solid-State Letters*, 2010, **13**, A115-A117.

233.   S. Hwang, S. M. Kim, S.-M. Bak, B.-W. Cho, K. Y. Chung, J. Y. Lee, W. Chang and E. A. Stach, *Acs Applied Materials & Interfaces*, 2014, **6**, 15140-15147.

234.   W.-S. Yoon, O. Haas, S. Muhammad, H. Kim, W. Lee, D. Kim, D. A. Fischer, C. Jaye, X.-Q. Yang, M. Balasubramanian and K.-W. Nam, *Sci. Rep.*, 2014, **4**.

235.   S. Hwang, W. Chang, S. M. Kim, D. Su, D. H. Kim, J. Y. Lee, K. Y. Chung and E. A. Stach, *Chemistry of Materials*, 2014, **26**, 1084-1092.

236.   S.-M. Bak, K.-W. Nam, W. Chang, X. Yu, E. Hu, S. Hwang, E. A. Stach, K.-B. Kim, K. Y. Chung and X.-Q. Yang, *Chemistry of Materials*, 2013, **25**, 337-351.

237.   B. Huang, X. H. Li, Z. X. Wang and H. J. Guo, *Materials Letters*, 2014, **131**, 210-213.

238.   S. N. Lim, W. Ahn, S. H. Yeon and S. Bin Park, *Electrochimica Acta*, 2014, **136**, 1-9.

239.   S. H. Lee, C. S. Yoon, K. Amine and Y. K. Sun, *Journal of Power Sources*, 2013, **234**, 201-207.

240.   W. M. Liu, G. R. Hu, K. Du, Z. D. Peng and Y. B. Cao, *Journal of Power Sources*, 2013, **230**, 201-206.

241.   M. A. Al-Maghrabi, J. S. Thorne, R. J. Sanderson, J. N. Byers, J. R. Dahn and R. A. Dunlap, *Journal of The Electrochemical Society*, 2012, **159**, A711-A719.

242.   J. S. Thorne, R. J. Sanderson, J. R. Dahn and R. A. Dunlap, *Journal of The Electrochemical Society*, 2010, **157**, A1085-A1091.

243.   M. S. Beal, B. E. Hayden, T. Le Gall, C. E. Lee, X. Lu, M. Mirsaneh, C. Mormiche, D. Pasero, D. C. A. Smith, A. Weld, C. Yada and S. Yokoishi, *ACS Combinatorial Science*, 2011, **13**, 375-381.

244.   C. R. Brown, E. McCalla, C. Watson and J. R. Dahn, *ACS*

Combinatorial Science, 2015, **17**, 381-391.
245. E. McCalla, A. W. Rowe, R. Shunmugasundaram and J. R. Dahn, *Chemistry of Materials*, 2013, **25**, 989-999.
246. E. McCalla, C. M. Lowartz, C. R. Brown and J. R. Dahn, *Chemistry of Materials*, 2013, **25**, 912-918.
247. G. H. Carey and J. R. Dahn, *ACS Combinatorial Science*, 2011, **13**, 186-189.
248. J. Lee, A. Urban, X. Li, D. Su, G. Hautier and G. Ceder, *Science*, 2014, **343**, 519-522.
249. R. Chen, S. Ren, M. Yavuz, A. A. Guda, V. Shapovalov, R. Witter, M. Fichtner and H. Hahn, *Physical Chemistry Chemical Physics*, 2015, **17**, 17288-17295.
250. N. Yabuuchi, M. Takeuchi, M. Nakayama, H. Shiiba, M. Ogawa, K. Nakayama, T. Ohta, D. Endo, T. Ozaki, T. Inamasu, K. Sato and S. Komaba, *Proceedings of the National Academy of Sciences*, 2015, **112**, 7650-7655.
251. R. Wang, X. Li, L. Liu, J. Lee, D.-H. Seo, S.-H. Bo, A. Urban and G. Ceder, *Electrochemistry Communications*, 2015, **60**, 70-73.
252. J. Lee, D.-H. Seo, M. Balasubramanian, N. Twu, X. Li and G. Ceder, *Energy & Environmental Science*, 2015, **8**, 3255-3265.
253. N. Yabuuchi, Y. Tahara, S. Komaba, S. Kitada and Y. Kajiya, *Chemistry of Materials*, 2016, **28**, 416-419.